

**NASA CONTRACTOR
REPORT**

NASA CR-1998



NASA CR-1998

0061270



LOAN COPY: RETURN TO
AFWL (DOUL)
KIRTLAND AFB, N. M.

**A DIGITAL COMPUTER STUDY
OF THE BUCKLING
OF SHALLOW SPHERICAL CAPS
AND TRUNCATED HEMISPHERES**

by William C. Stilwell and Robert E. Ball

Prepared by
NAVAL POSTGRADUATE SCHOOL
Monterey, Calif. 93940
for Langley Research Center



NATIONAL AERONAUTICS AND SPACE ADMINISTRATION • WASHINGTON, D. C. • JUNE 1972



0061270

1. Report No. NASA CR-1998	2. Government Accession No.	3. Recipient's Catalog No.	
4. Title and Subtitle A DIGITAL COMPUTER STUDY OF THE BUCKLING OF SHALLOW SPHERICAL CAPS AND TRUNCATED HEMISPHERES		5. Report Date June 1972	6. Performing Organization Code
		8. Performing Organization Report No.	
7. Author(s) William C. Stilwell and Robert E. Ball		10. Work Unit No.	
9. Performing Organization Name and Address Naval Postgraduate School Monterey, Calif. 93940		11. Contract or Grant No. L-16,438	
		13. Type of Report and Period Covered Contractor Report	
12. Sponsoring Agency Name and Address National Aeronautics and Space Administration Washington, D.C. 20546		14. Sponsoring Agency Code	
		15. Supplementary Notes	
16. Abstract <p>A study of the buckling of thin shells was conducted using a digital computer program for the geometrically nonlinear analysis of arbitrarily loaded shells of revolution. The objective was an evaluation of the program's applicability to bifurcation buckling and imperfection sensitivity analysis.</p> <p>Clamped spherical caps under pressure loading and clamped truncated hemispheres under axial tension were investigated. Buckling loads were determined for axisymmetric and nearly axisymmetric loads and are compared with previously published theoretical and experimental results. The sensitivity of the loaded shells to imperfections in load was determined and is compared with previously published analytical results based on geometric imperfections.</p> <p>The work was conducted under the auspices of the Department of Aeronautics of the Naval Postgraduate School, Monterey, California.</p>			
17. Key Words (Suggested by Author(s)) Buckling Shell analysis Nonlinear structural analysis Shells of revolution		18. Distribution Statement Unclassified - Unlimited	
19. Security Classif. (of this report) Unclassified	20. Security Classif. (of this page) Unclassified	21. No. of Pages 47	22. Price* \$3.00



TABLE OF CONTENTS

I.	INTRODUCTION	1
II.	DESCRIPTION OF THE COMPUTER PROGRAM	2
	A. COORDINATE SYSTEM	2
	B. METHOD OF SOLUTION	2
	C. MODIFIED PROGRAM	4
	D. PROGRAM INPUTS	6
III.	APPLICATIONS	7
	A. SNAP BUCKLING	7
	B. BIFURCATION BUCKLING	7
	C. IMPERFECTION SENSITIVITY	10
	D. SELECTION OF SHELL GEOMETRY	11
IV.	SPHERICAL CAP DESCRIPTION AND RESULTS	13
	A. GEOMETRY	13
	B. LOAD DESCRIPTION	13
	1. Axisymmetric	13
	2. Asymmetric	15
	C. BOUNDARY CONDITIONS	15
	D. PROCEDURES	15
	1. Uniform Pressure	16
	2. Partial Uniform Loading	16
	E. RESULTS	16
	1. Uniform Pressure	16
	a. Axisymmetric Snap Buckling	16
	b. Bifurcation Buckling	18
	c. Imperfection Sensitivity	23

2.	Partial Area Loading	27
a.	Axisymmetric Snap Buckling	27
b.	Bifurcation Buckling	29
c.	Imperfection Sensitivity	32
V.	TRUNCATED HEMISPHERE DESCRIPTION AND RESULTS	33
A.	GEOMETRY	33
B.	LOAD DESCRIPTION	33
1.	Axisymmetric	33
2.	Asymmetric	33
C.	BOUNDARY CONDITIONS	35
D.	PROCEDURES	35
E.	RESULTS	35
1.	Axisymmetric Behavior	35
2.	Bifurcation Buckling	38
a.	Shell A	38
b.	Shell B	43
3.	Imperfection Sensitivity	46
VI.	CONCLUSIONS	50
A.	FINAL LOADS AS BUCKLING LOADS	50
B.	AXISYMMETRIC SNAP BUCKLING	51
1.	Spherical Cap	51
2.	Truncated Hemisphere	51
C.	BIFURCATION BUCKLING	52
1.	Spherical Cap	52
2.	Truncated Hemisphere	52
D.	IMPERFECTION SENSITIVITY	52
1.	Spherical Cap Under Uniform Pressure	53
2.	Truncated Hemisphere Under Axial Tension	53

APPENDIX A - User Prepared Subroutines	55
APPENDIX B - Additions to Program for Linear Symmetric Solution	61
APPENDIX C - Additions to Program for Asymmetric Axial Load . .	65
LIST OF REFERENCES	66

LIST OF FIGURES

Figure		Page
1.	Types of nonlinear behavior that have an effect upon convergence	5
2.	Typical load-displacement curves for a shell that is sensitive to load imperfections	8
3.	Geometry of a clamped shallow spherical shell	14
4.	Axisymmetric displacement at station 24 versus load for a clamped spherical cap, $\lambda=8$	17
5.	Critical pressures for axisymmetric snap buckling of clamped spherical caps	19
6.	Variation of final load with ϵ for $\lambda=8$	20
7.	Asymmetric modal displacement, $N=4$, at station 24 versus load; $\lambda=8$, $\epsilon=.0005$	21
8.	Buckling mode shape for $N=4$, $\lambda=8$	22
9.	Modal displacement, as percentage of the total displacement, at station 24 versus the load, $\lambda=8$	24
10.	Critical pressures for bifurcation buckling of clamped spherical caps	25
11.	Sensitivity of spherical cap, $\lambda=8$, to load imperfections	26
12.	Final loads for the axisymmetric behavior of clamped spherical caps under very small finite area loading at the pole	28
13.	Displacement at the pole of a clamped spherical cap, $\lambda=12$, subjected to a small finite area load versus load	30
14.	Final loads for the axisymmetric and asymmetric behavior of a clamped spherical cap, $\lambda=12$, under finite area loading as determined by λ	31
15.	Geometry of the truncated hemisphere	34
16.	Axisymmetric, meridional displacements of Shell A under axial tension $P_o/Eh=1.325 \times 10^{-3}$	36

17.	Axisymmetric displacement, at station 8, versus load for Shell A	37
18.	Final loads for asymmetric behavior of Shell A subjected to axial tension with small asymmetric load, $\delta=.0001$	39
19.	Buckling, meridional mode shape, $N=40$, of Shell A subjected to axial tension with small asymmetric load, $\delta=.0001$	40
20.	Meridional mode shape, $N=15$, of Shell A subjected to axial tension with small asymmetric load, $\delta=.0001$	41
21.	Development of buckling mode shape, $N=40$, of Shell A subjected to an axial tension load in the vicinity of the critical load with small asymmetric load, $\delta=.0001$	42
22.	Final loads for asymmetric behavior of Shell B subjected to an axial tension with small asymmetric load, $\delta=.0001$	44
23.	Buckling, meridional mode shape, $N=70$, of Shell B subjected to an axial tension with small asymmetric pressure, $\epsilon=.001$	45
24.	Variation of final load with δ and ϵ for Shell B . . .	47
25.	Sensitivity of Shell B to load imperfections	48

TABLE OF SYMBOLS

a	a reference distance
E, E ₀	the modulus of elasticity of the shell and the reference modulus of elasticity respectively
H	the rise of the spherical cap; the distance from the boundary to the pole measured along the axis of revolution (see Fig. 3)
h, h ₀	the thickness of the shell and the reference thickness respectively
$[K_L^{(n)}]$	the square matrix associated with the linear terms in the n th set of equilibrium equations
$[K_{NL}^{(N)}]$	the square matrix associated with the nonlinear terms in the N th set of equilibrium equations
L	the rise of the truncated hemisphere; the distance from the equator to the final edge measured along the axis of revolution (see Fig. 15)
M _s	the meridional bending moment per unit length
n	the mode number, or the number of a term in the trigonometric expansion of the dependent variables and the number of a set of equilibrium equations
N	a specific value of n other than zero
N _L	a nondimensional axial load
N _s	the membrane force per unit length
P	an applied load in pounds
P*	a nondimensional applied load
P ₀	the axisymmetric applied axial load (see Fig. 15)
q	the axisymmetric applied pressure at a point on the shell
q ₀	the classical buckling pressure of a complete sphere
q ^(N)	the coefficient of the N th term in the trigonometric expansion of the applied pressure
{q ^{(n)}} }	a column matrix containing the coefficients of the n th term in the series expansion of the applied load

$\{q_{NL}^{(n)}\}$	a column matrix containing all of the nonlinear terms in the n^{th} set of equilibrium equations; the pseudo loads
Q_s	a transverse force per unit length
q_T	the total applied pressure load at a point on the shell
r	the normal distance of any point on the reference surface from the axis of revolution (see Fig. 3)
\bar{r}	the normal distance from the axis of revolution to the last point of applied pressure (see Fig. 3)
R_s, R_e	the radii of curvature in the s and e directions respectively
s	the meridional distance along a reference surface
S	the total meridional distance of the reference surface
U, V, W	the displacements in the s, e and ζ directions respectively
$W^{(n)}$	the displacement in the ζ direction in the n^{th} mode
$\{Z^{(n)}\}$	a column matrix containing the coefficients of the n^{th} term in the series expansion of the unknowns U, V, W and M_s
$\{Z_L^{(N)}\}, \{Z_{NL}^{(N)}\}$	the linear and nonlinear parts respectively of $\{Z^{(N)}\}$
δ	the nondimensional parameter governing the maximum magnitude of the applied asymmetric axial load
ϵ	the nondimensional parameter governing the maximum magnitude of the applied asymmetric pressure
ζ	the normal to the reference surface
e	the circumferential angle measured about the axis of revolution
λ	a nondimensional geometric parameter used to describe the spherical cap
$\bar{\lambda}$	a nondimensional loading parameter describing the area of loading on the spherical cap
ν	Poisson's ratio
σ_0	a reference stress
ϕ_0	the included angle of the truncated hemisphere measured from the equator to the final edge (see Fig. 15)
ϕ_s	the rotation of the meridian

I. INTRODUCTION

There are in existence several user-oriented digital computer programs for the static analysis of shells of revolution. A detailed discussion of most of these programs is given in Ref. 1. Of particular interest here is the program developed by Ball [Ref. 2] for the geometrically nonlinear analysis of arbitrarily loaded shells of revolution. This program is an equilibrium program; that is, it solves for the displacement and stress resultant fields for an arbitrary loading condition. Since geometric nonlinearities are included, the magnitude of load that leads to a condition of instability can be determined.

The utility of the program would be considerably enhanced if it could be used to determine bifurcation buckling loads and the behavior of the shell in the vicinity of the bifurcation load. This latter feature is often referred to as the imperfection sensitivity of the shell to the load. As a consequence, the objective of this study was to use the computer program to examine the buckling behavior of several shells subjected to axisymmetric and nearly axisymmetric loads. It was anticipated that an examination of the effects of the small asymmetric perturbations upon the stability of the shell would disclose the bifurcation buckling load and provide a quantitative evaluation of the imperfection sensitivity of the shell to the load.

II. DESCRIPTION OF THE COMPUTER PROGRAM

The computer program used in this study is a modified version of the program described in Ref. 2. The program is capable of analyzing thin, linearly elastic shells of revolution subjected to arbitrary loads and temperature distributions. It solves Sanders' nonlinear field equations for the conditions of small strains and moderately small rotations.

A. COORDINATE SYSTEM

The coordinate system used to locate points within the shell is s , θ and ζ , where s is the meridional distance along a reference surface, ζ is the normal to the surface and θ is the circumferential angle measured about the axis of revolution.

B. METHOD OF SOLUTION

The governing partial differential equations are reduced to four second order ordinary differential equations by expanding all dependent variables in trigonometric series in the θ direction. Each of the nonlinear terms, which are products of series, is further expanded into a single series. The coefficients of like trigonometric arguments are then grouped to form coupled sets of ordinary differential equations. The sets of differential equations are uncoupled by treating the nonlinear terms as known quantities or pseudo loads. A finite difference formulation is employed for the meridional derivatives of the variables. This leads to sets of algebraic equations of the form

$$\begin{bmatrix} K \\ L \end{bmatrix}^{(n)} \{ Z^{(n)} \} = \{ q^{(n)} \} + \{ q_{NL}^{(n)} \} \quad (1)$$

The square matrix $[K_L^{(n)}]$ is a banded matrix associated with the linear portion of the governing equations. The unknown variables in the column matrix $\{Z^{(n)}\}$ are the coefficients of the n^{th} term in the series expansions of U , V , W and M_s at each finite difference station. The variables U , V and W are the displacements in the s , θ and ζ directions respectively, and M_s is the meridional bending moment per unit length. The applied loads in the n^{th} mode are contained in the column matrix $\{q^{(n)}\}$, and the column matrix $\{q_{NL}^{(n)}\}$ contains all of the nonlinear terms. There is one such matrix equation for every value of n used in the trigonometric expansions of the dependent variables.

An elimination procedure is used to solve each set of equations for the actual loads plus an estimate of the pseudo loads. The nonlinear terms are then recalculated, using the new solution, and entered as revised pseudo loads. All of the sets of equations are then solved again, and this procedure is repeated until two consecutive solutions in each mode differ by less than a specified amount. This method of solution is referred to as the Jacobi method.

A load-displacement history is obtained by incrementing the applied loads in equal load steps until the number of iterations required to achieve convergence in any mode exceeds a prescribed limit. The load increment is then reduced by a factor of five, and the procedure continues until a prescribed number of load steps or a prescribed number of load step reductions have been made.

Since the method of solution is based on a nonlinear pseudo load approach, the shell reacts equally, in a linear fashion, to any change in either the applied load or the pseudo load. Thus, failure of the solution to converge in any mode can be attributed to two types of nonlinear behavior. Both types are illustrated in Fig. 1. The existence

of a maximum or an inflection point on the softening load-deflection curve A represents a type of behavior for which a solution can be obtained only below the point of zero or nearly zero slope. On the other hand, the existence of a stiffening nonlinearity, as illustrated by curve B of Fig. 1, can also cause a convergence failure whenever the slope becomes too steep. Thus, in general, it is necessary to examine the load-displacement behavior of the shell in order to determine the cause of the convergence failure.

C. MODIFIED PROGRAM

The program used in this study was a modified version containing revisions made by personnel at the NASA Langley Research Center and by the original author. The main difference between the modified program and the version given in Ref. 2 is the manner in which core storage is allocated for the solution vector. The solution vector was changed from a three dimensional array to a two dimensional array, allowing any combination of meridional and circumferential unknowns to be specified. The product of the number of meridional stations and the number of terms in the trigonometric expansions must be less than 201, and the maximum number of terms in the trigonometric expansions must be less than 11.

The difference in storage allocation necessitated changes in the method of handling the geometry, the inplane and bending stiffnesses, and the loads. The subroutine STIF was replaced by the subroutine BDB; subroutine PTLOAD was replaced by two subroutines, PLOAD and TLOAD; and subroutine ACOEF was eliminated. In addition, two subroutines, HJ and EFG, given in Ref. 3, were substituted for the original subroutines HJ and EFG.

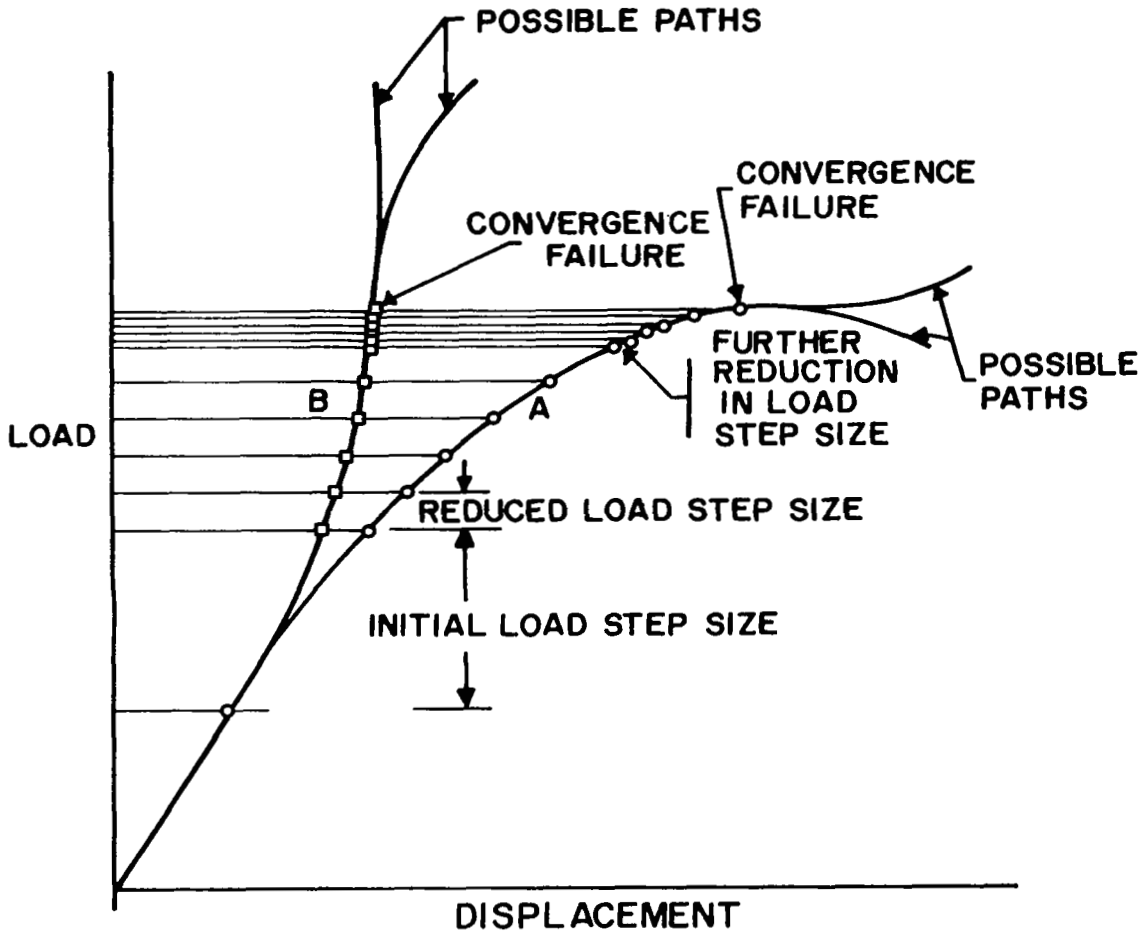


Fig. 1 Types of nonlinear behavior that have an effect upon convergence.

An additional change has been made in the test for convergence. Convergence was set such that the difference in two successive modal solutions, at every station, must be less than the convergence criterion times the maximum solution in that mode, provided the maximum solution is greater than 10^{-6} . The test for convergence is not required when the maximum solution is less than 10^{-6} . This change was made to provide converged, accurate solutions in fewer iterations.

Finally, the subroutine OUTPUT has been modified in order to present the data in more compact form; the COMMON and DIMENSION statements have been changed to allow the compilation of the program in any order; and several "bugs" were detected and eliminated.

The modified program occupies approximately 146,000 bytes or about 36,500 words on the IBM 360/67.

D. PROGRAM INPUTS

The user-prepared subroutines BDB, GEOM and PLOAD, describing the shell stiffness, geometry and applied loads, for the shells covered in this study are given in Appendix A. The important parameters that can be varied for a given shell geometry are; number of points, number of modes required in the solution, number of modes used to describe the load, boundary conditions, loading condition, convergence criterion, load step size, number of load step reductions and number of iterations.

III. APPLICATIONS

The program was used to solve for the response of several shells subjected to axisymmetric and nearly axisymmetric loads. Figure 2 presents three load-displacement curves that are typical of the types of axisymmetric behavior predicted by the program for a shell that is imperfection sensitive.

A. SNAP BUCKLING

Axisymmetric snap buckling is illustrated by curve E of Fig. 2, and the application of the program to determine the snap buckling load is fairly straight forward. The program, as previously discussed, will not be able to find a converged solution in the vicinity of the snap buckling load.

B. BIFURCATION BUCKLING

The program, as currently formulated, cannot be used to solve the classical eigenvalue problem for the bifurcation load of an axisymmetrically loaded shell. However, it is possible to introduce a small asymmetry in the load and to determine the unsymmetric buckling behavior for the nearly axisymmetric load. In the limit, as the asymmetry of the load approaches zero, the asymmetric buckling load should approach the bifurcation load. This conclusion is based upon the following two mode analysis.

Consider that the applied load consists of an axisymmetric part $\{q^{(0)}\}$ and a very small asymmetric part $\{q^{(N)}\}$. It can be shown that due to the load and modal coupling there will be displacements in the modes 0, N, 2N, 4N, 6N, etc.. For this analysis only the two lowest modes

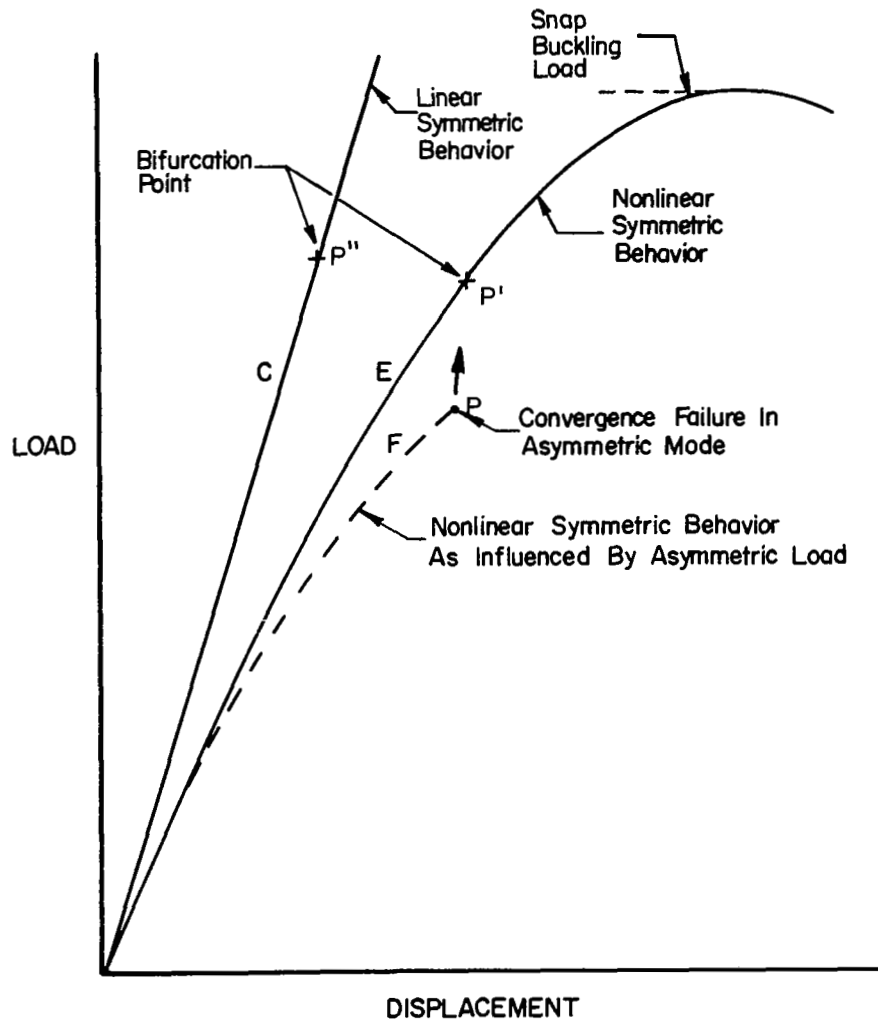


Fig. 2. Typical load displacement curves for a shell that is sensitive to load imperfections.

are considered to be significant. According to equation (1), the matrix equations for these two modes are

$$\left[K_L^{(0)} \right] \{ Z^{(0)} \} = \{ q^{(0)} \} + \{ q_{NL}^{(0)} \} \quad (2a)$$

$$\left[K_L^{(N)} \right] \{ Z^{(N)} \} = \{ q^{(N)} \} + \{ q_{NL}^{(N)} \} \quad (2b)$$

As a result of modal coupling $\{ q_{NL}^{(0)} \}$ and $\{ q_{NL}^{(N)} \}$ are functions of both $\{ Z^{(0)} \}$ and $\{ Z^{(N)} \}$. The behavior of the axisymmetric mode is illustrated by curve F in Fig. 2. Note that the difference between curve E and curve F is due to the presence of $\{ Z^{(N)} \}$ in the nonlinear terms of equation (2a). Point P on curve F represents the maximum load for which a converged solution of equation (2b) can be obtained.

The nonlinear terms in equation (2b) can be given in the form

$$\{ q_{NL}^{(N)} \} = \left[K_{NL}^{(N)} \right] \{ Z^{(N)} \} \quad (3)$$

where $\left[K_{NL}^{(N)} \right]$ is a function of $\{ Z^{(0)} \}$ only. The solution vector $\{ Z^{(N)} \}$ can be separated into a linear part $\{ Z_L^{(N)} \}$ and a nonlinear part $\{ Z_{NL}^{(N)} \}$ such that

$$\{ Z^{(N)} \} = \{ Z_L^{(N)} + Z_{NL}^{(N)} \} \quad (4a)$$

where $\{ Z_L^{(N)} \}$ is defined by

$$\left[K_L^{(N)} \right] \{ Z_L^{(N)} \} = \{ q^{(N)} \} \quad (4b)$$

Substituting equations (3), (4a) and (4b) into equation (2b) leads to

$$\left[K_L^{(N)} \right] \{ Z_{NL}^{(N)} \} = \left[K_{NL}^{(N)} \right] \{ Z_L^{(N)} + Z_{NL}^{(N)} \} \quad (5a)$$

When $\{ q^{(N)} \}$ is approximately zero, $\{ Z_L^{(N)} \}$ is very small.

If

$$\{z_{NL}^{(N)}\} \gg \{z_L^{(N)}\} \quad (5b)$$

then equation (5a) becomes

$$[K_L^{(N)}] \{z_{NL}^{(N)}\} \approx [K_{NL}^{(N)}] \{z_{NL}^{(N)}\} \quad (5c)$$

Equation (5c) is an approximation to the formulation of an eigenvalue problem and the displacements contained in $\{z_{NL}^{(N)}\}$ define the buckling mode shape. The magnitude of $\{z_{NL}^{(N)}\}$ is negligible until the applied load approaches the value at point P in Fig. 2. Thus, when $\{z_L^{(N)}\}$ is negligible, curve F will nearly coincide with curve E and P will approach P', the bifurcation point.

In some instances, a linear solution for the axisymmetric mode is desirable. This is usually referred to as a linear prebuckling analysis. For this condition $\{z^{(0)}\}$ is a linear function of the applied load, and thus $[K_{NL}^{(N)}]$, which is a function of $\{z^{(0)}\}$ only, is also a linear function of the applied load. Therefore, equation (5c) becomes an approximation to a linear eigenvalue problem. Curve C in Fig. 2 illustrates a typical linear axisymmetric behavior with the bifurcation point denoted by point P''. Several changes had to be made to the program in order to obtain a linear solution in the axisymmetric mode and a nonlinear asymmetric solution. These changes are presented in Appendix B.

C. IMPERFECTION SENSITIVITY

An imperfection sensitive shell is one for which the buckling load is reduced due to the presence of asymmetric imperfections¹. Therefore,

¹The sensitivity of a shell is a function of the loading condition.

curve F of Fig. 2 is a typical illustration of an imperfection sensitive shell since P falls below P'. For a shell that is insensitive to imperfections, P is above P'.

In a two mode analysis, the presence of the asymmetric response will have some influence on the response of the axisymmetric mode since it appears in $\{q_{NL}^{(0)}\}$. The axisymmetric mode will affect the response in the asymmetric mode through $[K_{NL}^{(N)}]$. Thus, the sensitivity of a given shell and loading condition must be examined in two parts;

- (1) the nature of the effect of $\{z^{(N)}\}$ on $\{z^{(0)}\}$
- (2) The nature of the effect of $\{z^{(0)}\}$ on $\{z^{(N)}\}$

As a consequence of this interaction, the program cannot be used to determine imperfection sensitivity when a linear axisymmetric solution is employed since item (1) is eliminated.

Application of the program to determine the sensitivity of a shell is limited to the extent that the asymmetric imperfections can only be introduced by applying an asymmetric load. Thus, the imperfections are not stress free as is usually assumed; nevertheless, if the asymmetric load is small the associated stresses will be small.

D. SELECTION OF SHELL GEOMETRY

In order to establish the ability of the program to determine bifurcation loads and the sensitivity of the shell to these loads, the results from the program must be compared with previously published analytical and experimental data. Thus, the spherical cap was selected as one shell geometry to investigate since numerous results, both theoretical and experimental, are available for a wide variety of loading conditions. Furthermore, previous investigations indicate that the spherical cap exhibits all of the traits desired; that is,

the symmetric behavior is a snap buckling phenomenon, bifurcation loads exist, for various size caps, below the symmetric snap load, and the shell is sensitive to imperfections over a wide range of loading conditions.

Another type of spherical shell was selected for which new results were obtained. This was the truncated hemisphere under axial tension. The experimental results that are available for this shell do not agree with the theoretical results. Imperfection sensitivity was suspected to be the cause of the discrepancy.

IV. SPHERICAL CAP DESCRIPTION AND RESULTS

A. GEOMETRY

The geometry of the spherical cap is shown in Fig. 3 and can be specified by a nondimensional geometric parameter λ , where

$$\lambda = 2 [3(1-\nu^2)]^{1/4} (H/h)^{1/2} \quad (6)$$

and H is the rise of the cap, h is the thickness and ν is Poisson's ratio. For all shells considered:

Radii of curvature, R_s, R_o	= 250 in
Thickness, h	= .25 in
Modulus of elasticity, E	= 30×10^6 psi
Poisson's ratio, ν	= .3

B. LOAD DESCRIPTION

The classical buckling pressure of a complete sphere is

$$q_o = \frac{2E}{\sqrt{3(1-\nu^2)}} (h/R_s)^2 \quad (7)$$

1. Axisymmetric

A uniform load q was applied to the shell from the pole out to \bar{r} as shown in Fig. 3.

A nondimensional load parameter $\bar{\lambda}$ was used to describe the area of loading, where

$$\bar{\lambda} = [12(1-\nu^2)]^{1/4} (\bar{r}/h)(h/R_s)^{1/2} \quad (8)$$

If the approximation $H = r_o/2R_s$ is substituted into equation (6), then equation (8) can be expressed as

$$\bar{\lambda} = \frac{\bar{r}}{r_o} \lambda \quad (9)$$

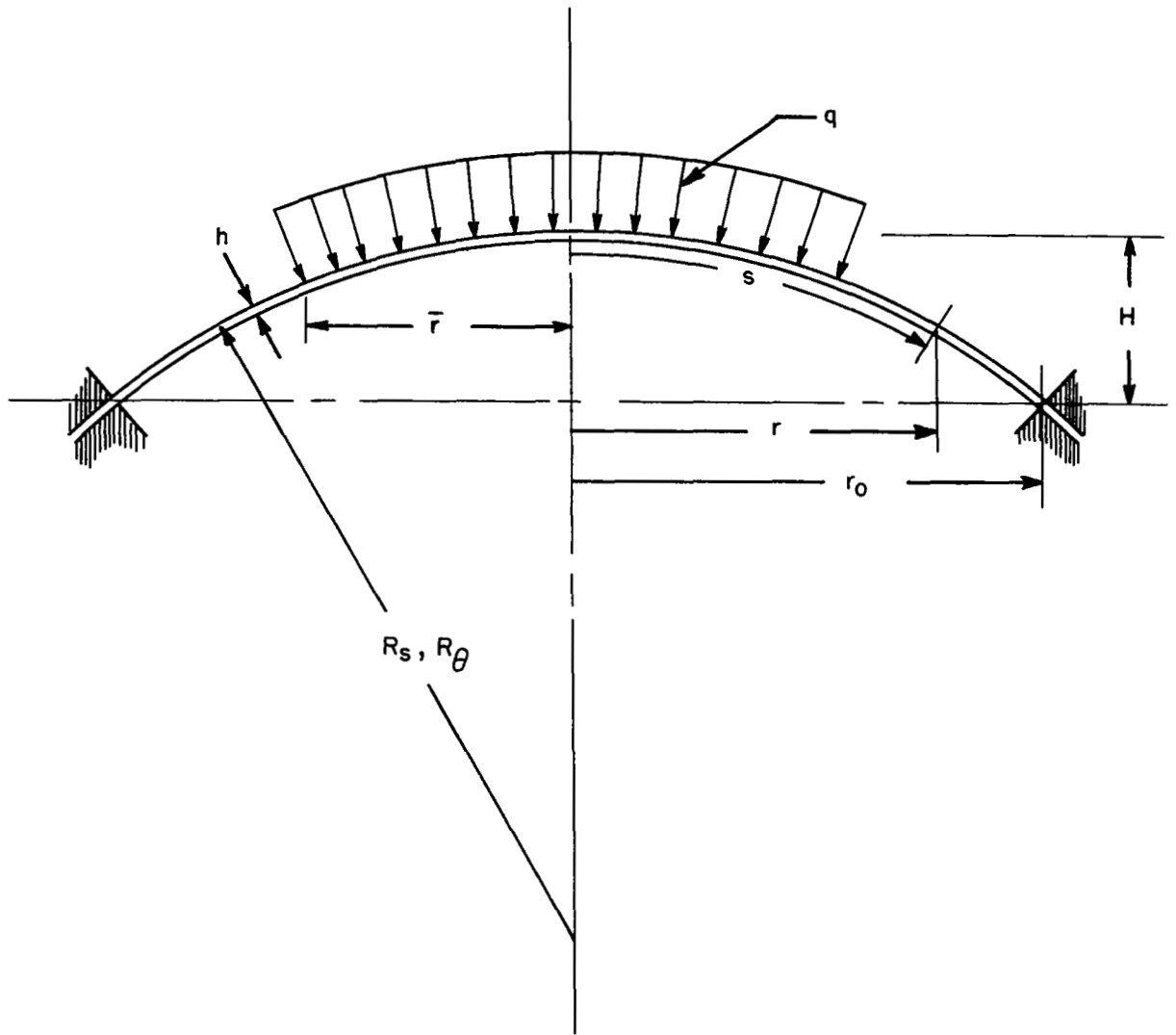


Fig. 3 Geometry of a clamped shallow spherical shell

For a small finite area load, approximating a point load, a dimensionless load parameter P^* was used, where

$$P^* = \frac{PR_s}{Eh^3} \quad (10)$$

and

$$P = \pi \bar{r}^2 q \quad (11)$$

where \bar{r} is equal to the distance between the pole and the first finite difference station.

2. Asymmetric

An asymmetric load was defined in one mode as

$$q^{(N)} = \epsilon q \quad (12)$$

where ϵ is a very small number. Thus, the nearly axisymmetric load is given by

$$q_T = q[1 + \epsilon \cos(N\theta)] \quad (13)$$

C. BOUNDARY CONDITIONS

The first station was at the pole and was handled internally within the program. The final edge was clamped and the boundary conditions are

$$U = V = W = \Phi_s = 0 \quad (14)$$

where Φ_s is the rotation of the meridian.

D. PROCEDURES

The axisymmetric and asymmetric behavior of the spherical cap was determined for both uniform pressure and partial uniform loading for several values of λ . In the majority of cases, forty stations were used along the meridian. The exception to this was the investigation of the axisymmetric snap buckling due to a uniform pressure. For $10 \leq \lambda \leq 16$,

80 stations were used; and for $\lambda > 16$, 100 stations were used. A stringent convergence criterion of .002 was used in all cases.

1. Uniform Pressure

For uniform pressure, $\bar{\lambda} = \lambda$. The symmetric behavior was examined first in order to establish the axisymmetric snap buckling pressures over a wide range of λ . One value of λ was then selected for full examination of the behavior under asymmetric load. The effect of varying ϵ over a wide range was examined and the degree of sensitivity estimated. A value of ϵ was selected for use in subsequent analysis of the bifurcation pressures. The final loads approximating the minimum bifurcation pressures were obtained for various values of λ .

2. Partial Uniform Loading

An investigation was made for the minimum value of $\bar{\lambda}$, approximating a point load, over a wide range of λ . The final loads were then obtained for axisymmetric snap buckling at various values of $\bar{\lambda}$ for one value of λ . Once the symmetric behavior had been obtained, very small asymmetric loads were introduced and an approximation obtained for the bifurcation loads as a function of $\bar{\lambda}$ at one value of λ . For small values of $\bar{\lambda}$, a linear symmetric solution was used.

E. RESULTS

1. Uniform Pressure

a. Axisymmetric Snap Buckling

The load-displacement curve at the 24th station for $\lambda=8$ is shown in Fig. 4. The transverse displacement at station 24 was the maximum displacement, and the nonlinear effects at this station were representative of the overall behavior. The load-displacement curve indicates the existence of a nearly zero slope which is indicative of

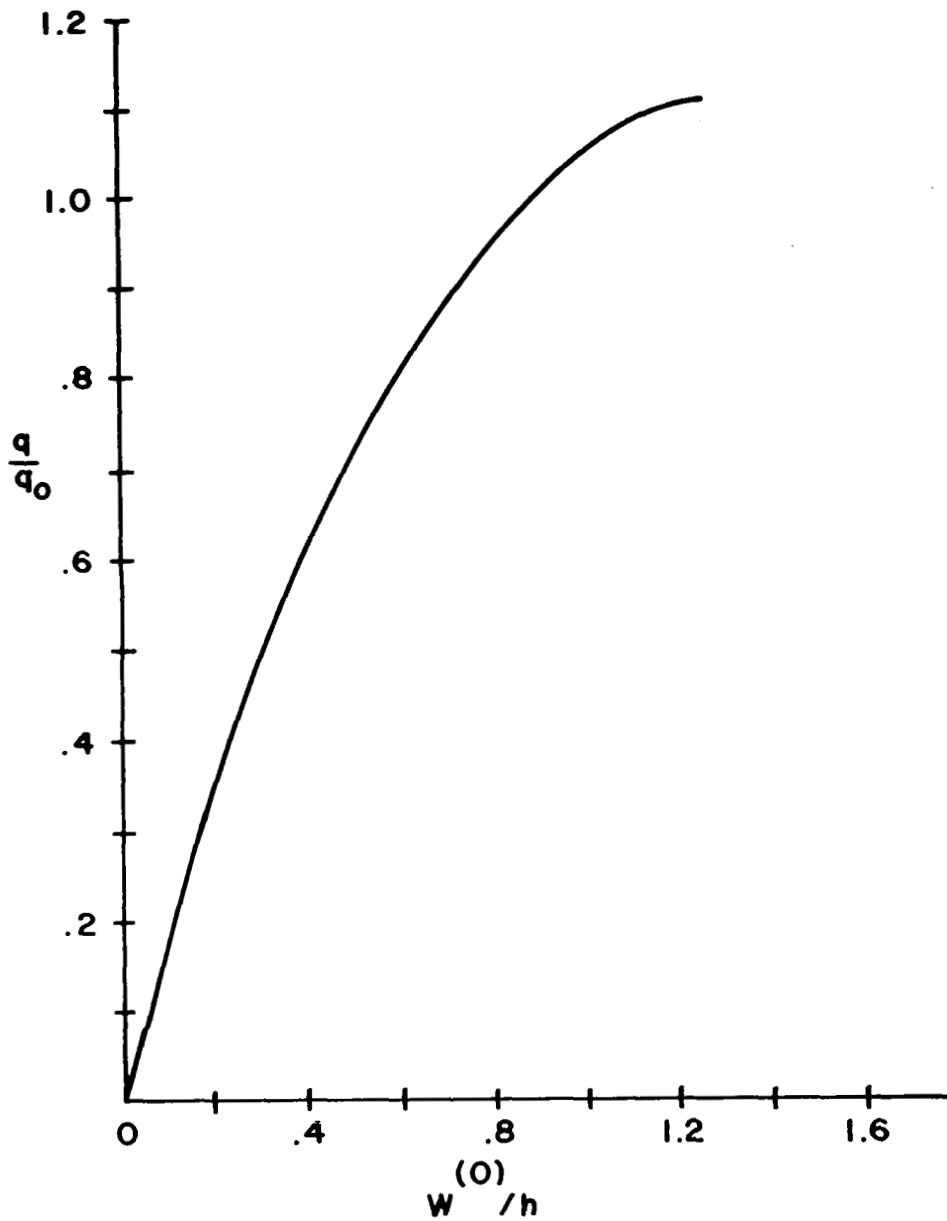


Fig. 4 Axisymmetric displacement at station 24 versus load for a clamped spherical cap, $\lambda = 8$.

snap buckling. Consequently, the final load is considered to be the critical pressure for axisymmetric snap buckling under a uniform pressure for $\lambda=8$.

Figure 5 shows the final loads obtained for several values of λ . The results of Weinitschke [Ref. 4] and Huang [Ref. 5] are also presented in Fig. 5.

b. Bifurcation Buckling

The effect of the nearly axisymmetric load given by equation (13) for $N=4$ was obtained for $\lambda=8$. According to Refs. 4 and 5, mode four is the critical mode number for this case. Figure 6 shows the final load as a function of ϵ . Note that as ϵ approaches zero, the final load asymptotically approaches a limiting value. Figure 7 shows the displacement in mode four at station 24 versus the load for $\epsilon = .0005$. The curve strongly indicates a region of zero slope at the final load and convergence failure is attributed to the asymmetric behavior. Furthermore, the nonlinear effects are definitely limited to a narrow load range near the final load. The ratio of nonlinear to linear displacements² at the final load were found to be of the order of 100 to 1, and the linear displacements were negligible. Thus, all of the requirements for a bifurcation analysis given in Section III.B. are satisfied, and the final load for $\epsilon = .0005$ is considered to be a close approximation to the bifurcation load. Figure 8 is a plot of the normalized, nonlinear modal displacements versus the nondimensional, normal distance from the axis and is the buckling mode shape. Also shown in Fig. 8 is the buckling mode shape obtained by Huang for $\lambda=9$.

²The final linear displacements were computed using the initial solution at the first load step.

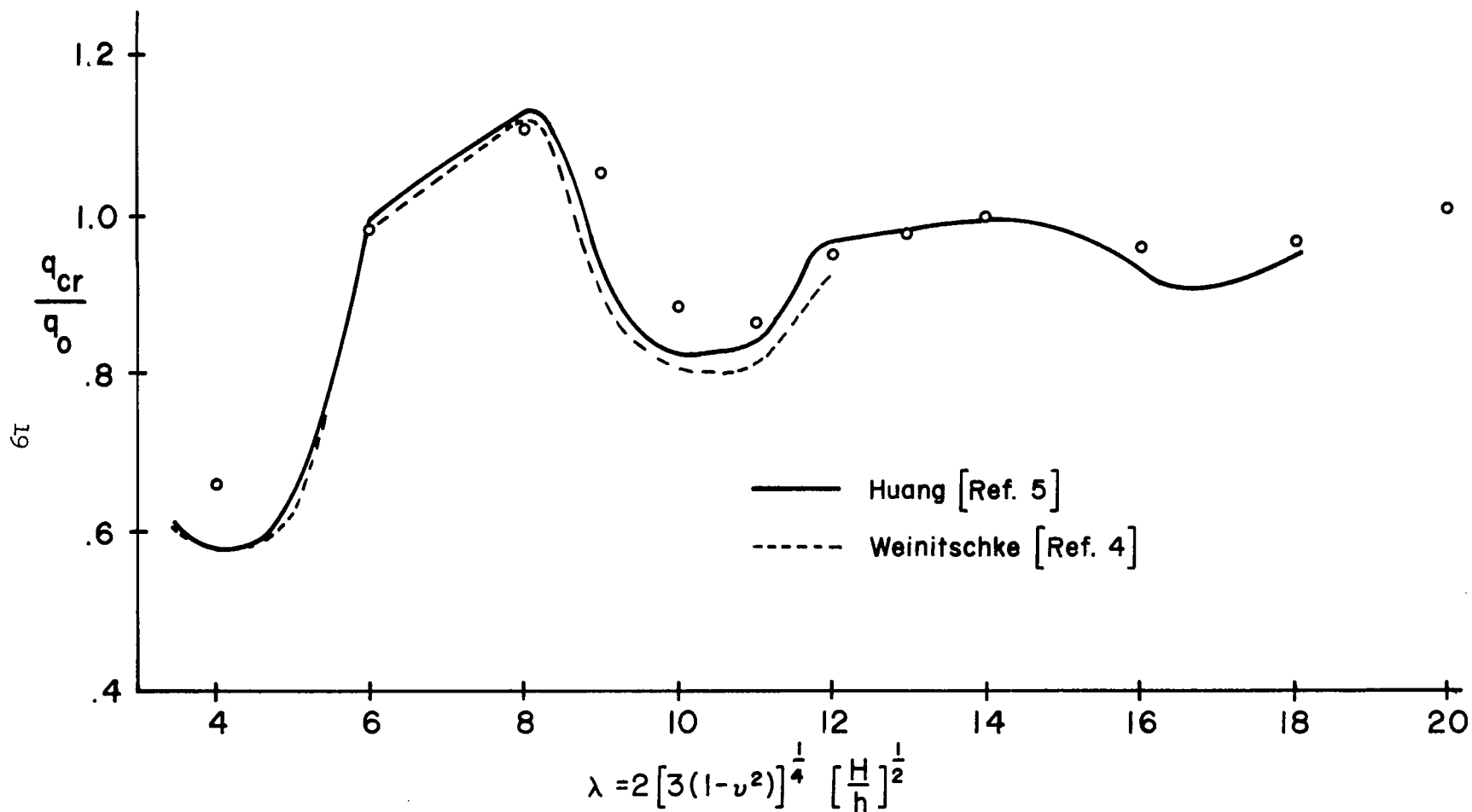


Fig. 5 Critical pressures for axisymmetric snap buckling of clamped spherical caps.

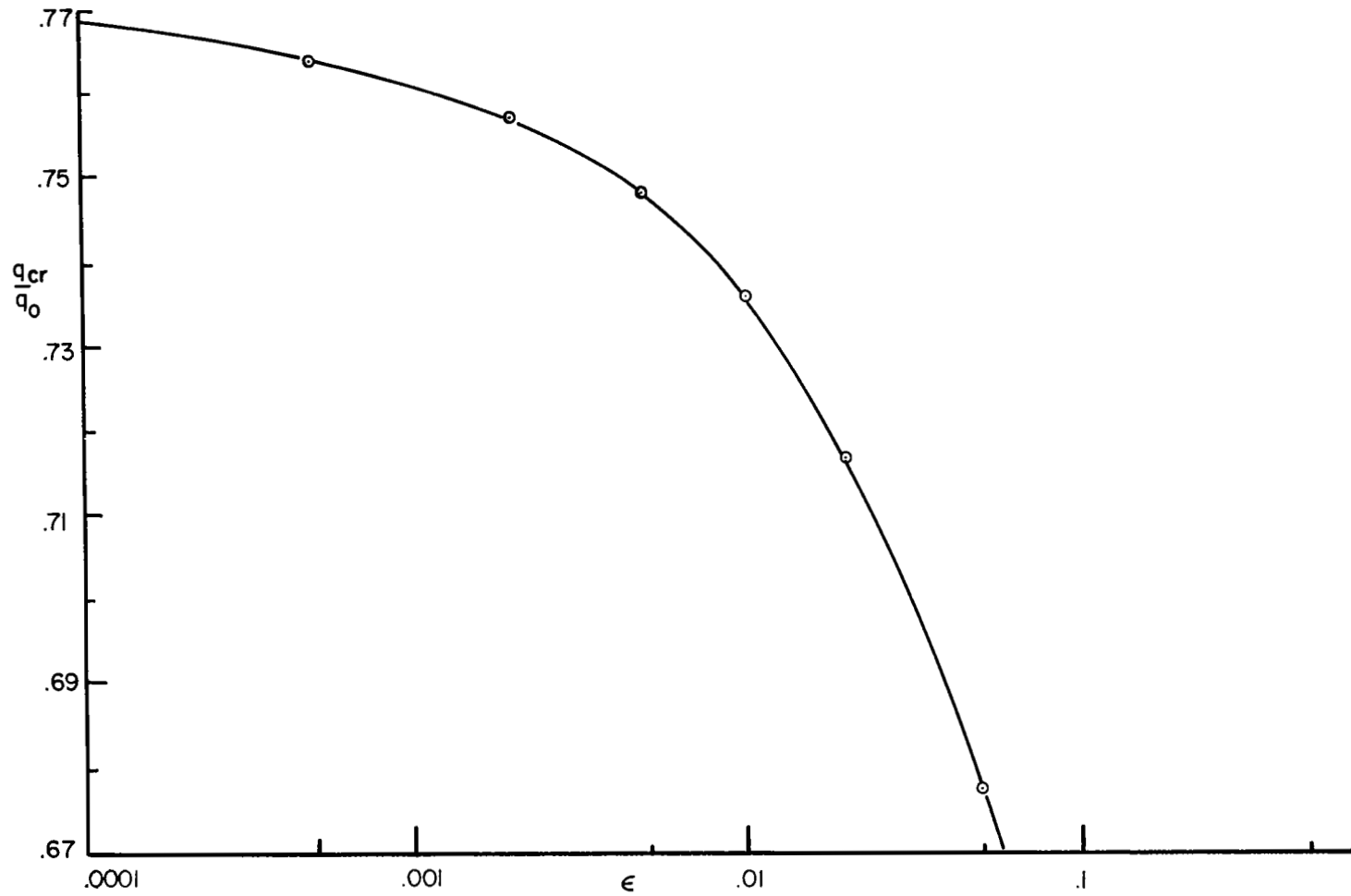


Fig. 6 Variation of final load with ϵ for $\lambda=8$

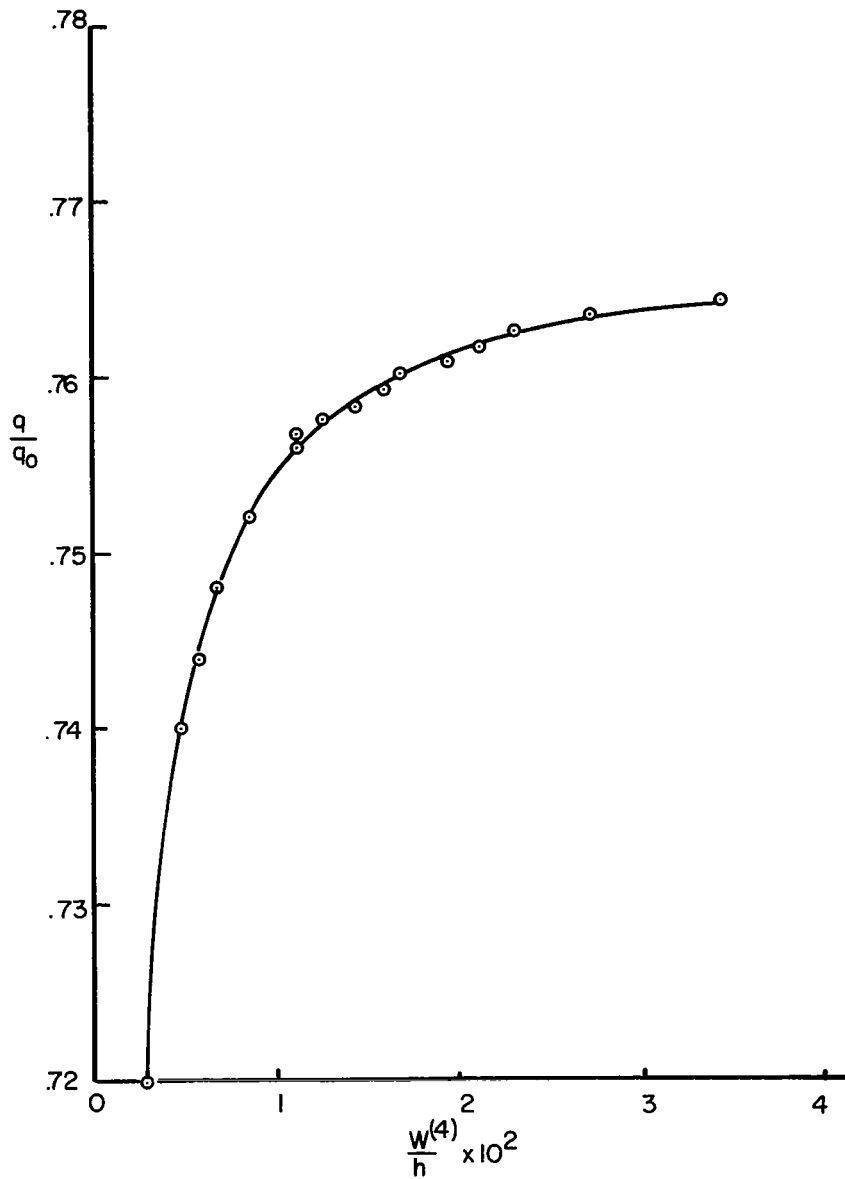


Fig. 7 Asymmetric modal displacement, $N=4$,
at station 24 versus load, $\lambda=8$, $\epsilon=.0005$

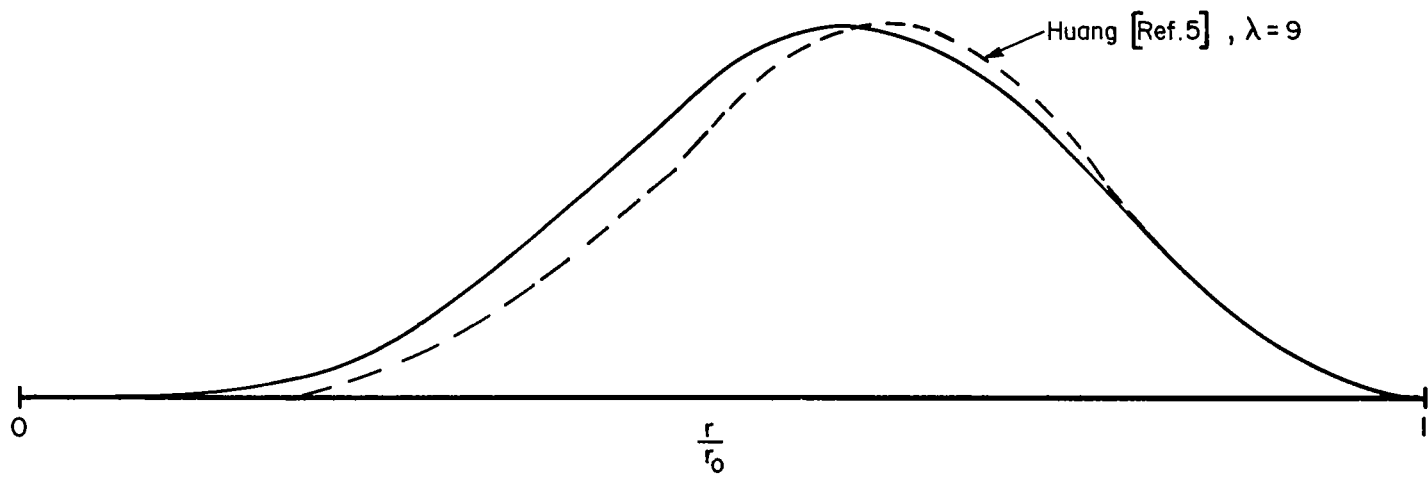


Fig. 8 Buckling mode shape for $N=4$, $\lambda=8$

When the critical mode number is unknown, the number of computer runs necessary to determine the critical mode number and the bifurcation load can be reduced by introducing additional modes in the solution. For example, for $\lambda=8$, an asymmetric load was introduced in mode one, with $\epsilon = .05$, and a solution was obtained in modes zero, one, two, three and four. Figure 9 shows the resultant asymmetric modal displacements at station 24 as a percentage of the total displacement versus the load. Note that the same softening characteristic present in Fig. 7 exists for modes three and four³. The failure of the solution to converge can be attributed to either mode three or four, since a zero slope is indicated by both. The final load is within 5% of the value obtained using a two mode solution. Thus, Fig. 9 illustrates the ability of a multimode analysis to obtain a first cut approximation to the bifurcation load and critical mode.

Results were obtained for approximate bifurcation loads at several other values of λ by selecting the critical modes as given in Ref. 5 and using a two mode solution with $\epsilon = .0002$. Figure 10 gives the final loads and critical mode numbers versus λ . Also shown in Fig. 10 are the bifurcation loads obtained by Huang.

c. Imperfection Sensitivity

As discussed in Section III.C., an imperfection sensitive shell is one for which the buckling load is reduced due to the presence of asymmetric imperfections. Figure 11 presents the load-displacement curves for the axisymmetric mode at station 24 for $\lambda=8$ and several values of ϵ . Note that as ϵ is increased the final load is decreased.

³According to Refs. 4 and 5, the bifurcation load for mode three is only slightly higher than that for mode four when $\lambda=8$.

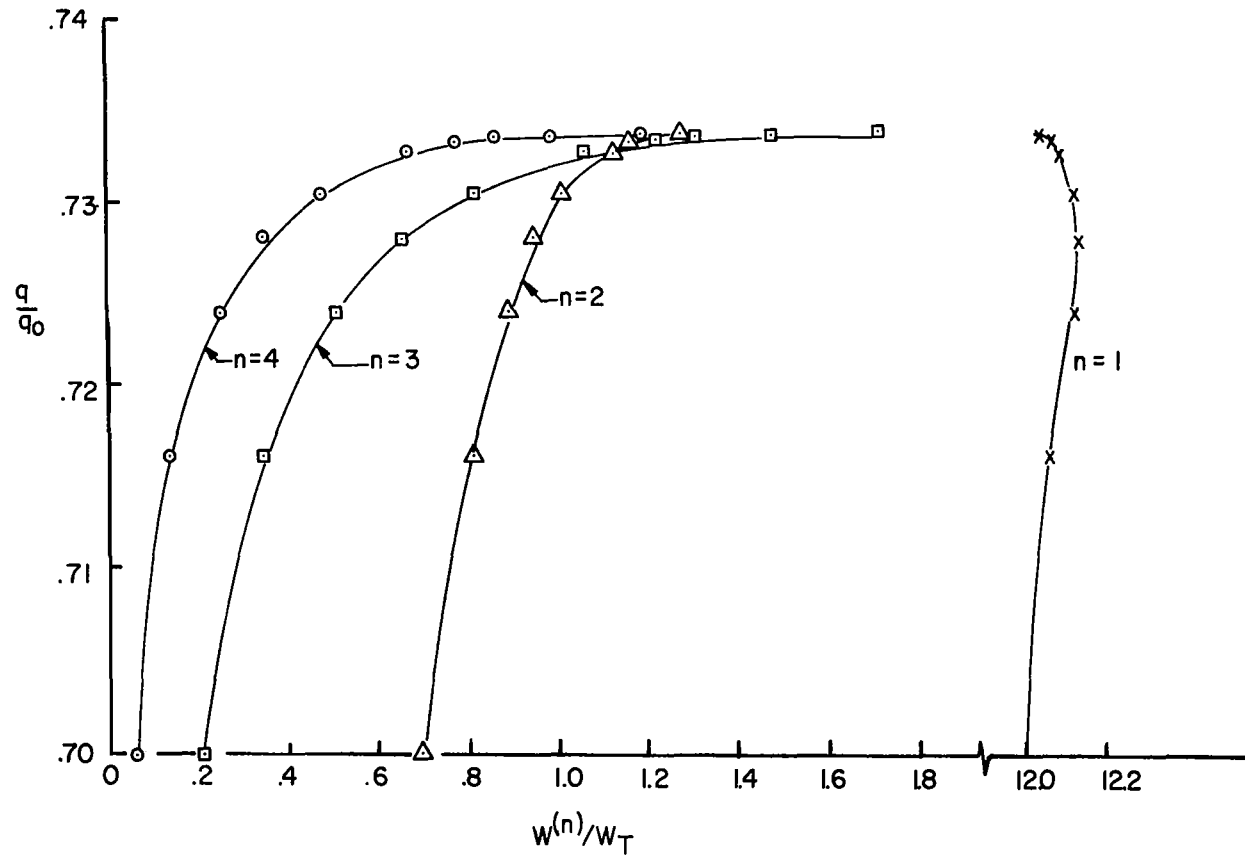


Fig. 9 Modal displacement, as percentage of the total displacement, at station 24 versus the load, $\lambda=8$

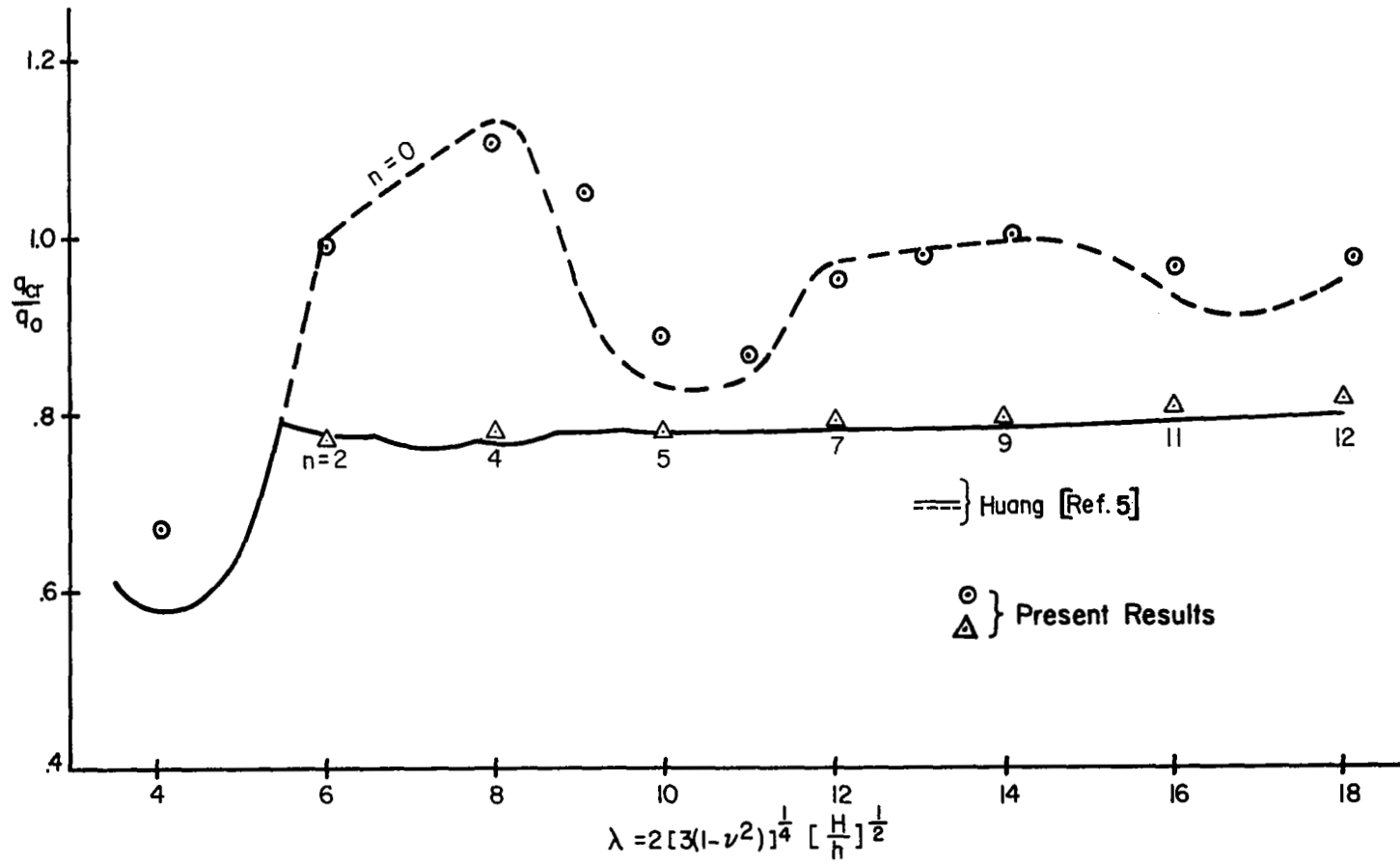


Fig.10 Critical pressures for axisymmetric snap buckling and bifurcation buckling of clamped spherical caps

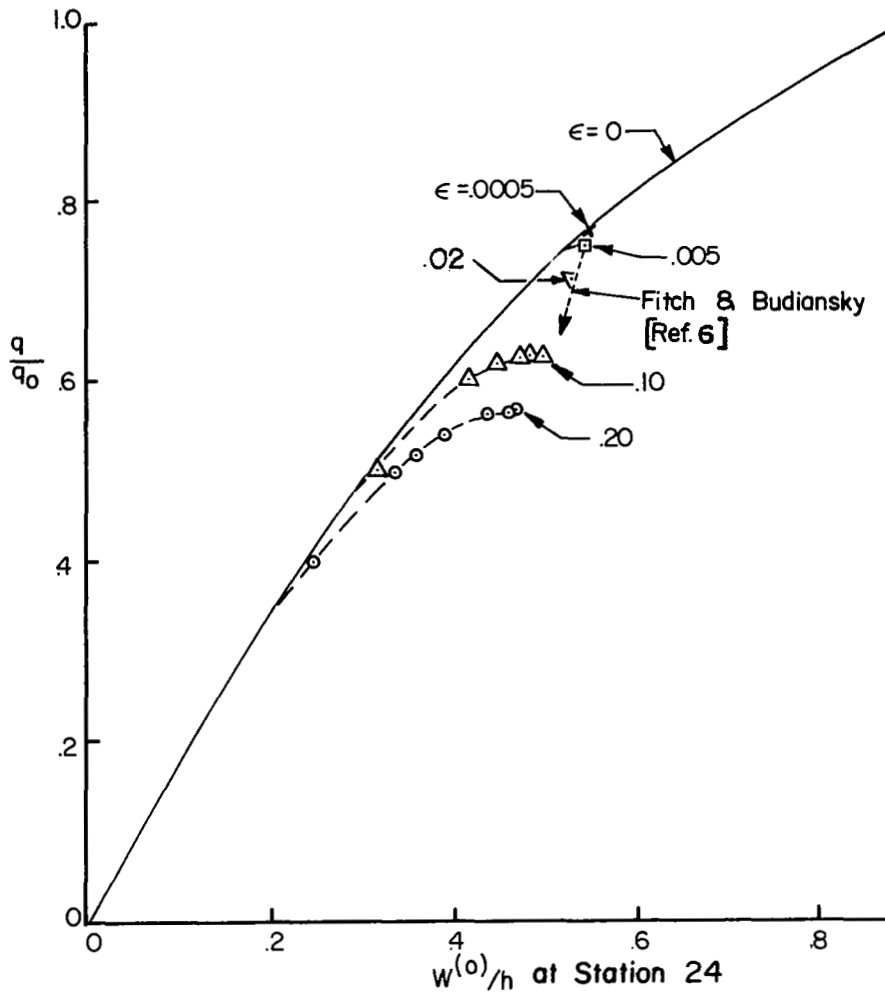


Fig. 11 Sensitivity of spherical cap, $\lambda=8$, to load imperfections

Thus, this shell appears to be imperfection sensitive for the uniform pressure loading condition. Fitch and Budiansky [Ref. 6] have conducted a study of the buckling and postbuckling behavior of spherical caps, subjected to centrally distributed pressure, based on Koiter's initial postbuckling theory. They found the shell $\lambda=8$ to be imperfection sensitive to the uniform pressure. They also predicted the initial slope of the bifurcation branch of the equilibrium path on a load-displacement plot. The predicted slope for the shell $\lambda=8$, subjected to uniform pressure, is given in Fig. 11⁴.

2. Partial Area Loading

a. Axisymmetric Snap Buckling

The final loads obtained for the axisymmetric behavior of the spherical cap under a small finite area load, approximating a point load at the pole, are shown in Fig. 12. Experimental results given by Penning and Thurston [Ref. 7] and Penning [Ref. 8] for axisymmetric snap buckling due to a small finite area load are also presented in Fig. 12. The experimental load-displacement curves for $\lambda > 15$ show a well-defined, abrupt discontinuity in the displacement at the pole, and the slope of the curve after the snap is somewhat less than the initial slope. Below a value of $\lambda=15$, the experimental results show no axisymmetric snap⁵, but a large majority of the load-displacement curves show significant decreases

⁴The load-displacement plot used by Fitch and Budiansky is based on an average deflection parameter. The load-displacement plot shown in Fig. 11 is based on the maximum displacement. The assumption is made that the rate of change of the average deflection parameter is essentially the same as the rate of change of the maximum displacement.

⁵Three atypical shells with poor radial geometry did buckle at loads somewhat below $P^*=2.0$, [Ref. 8].

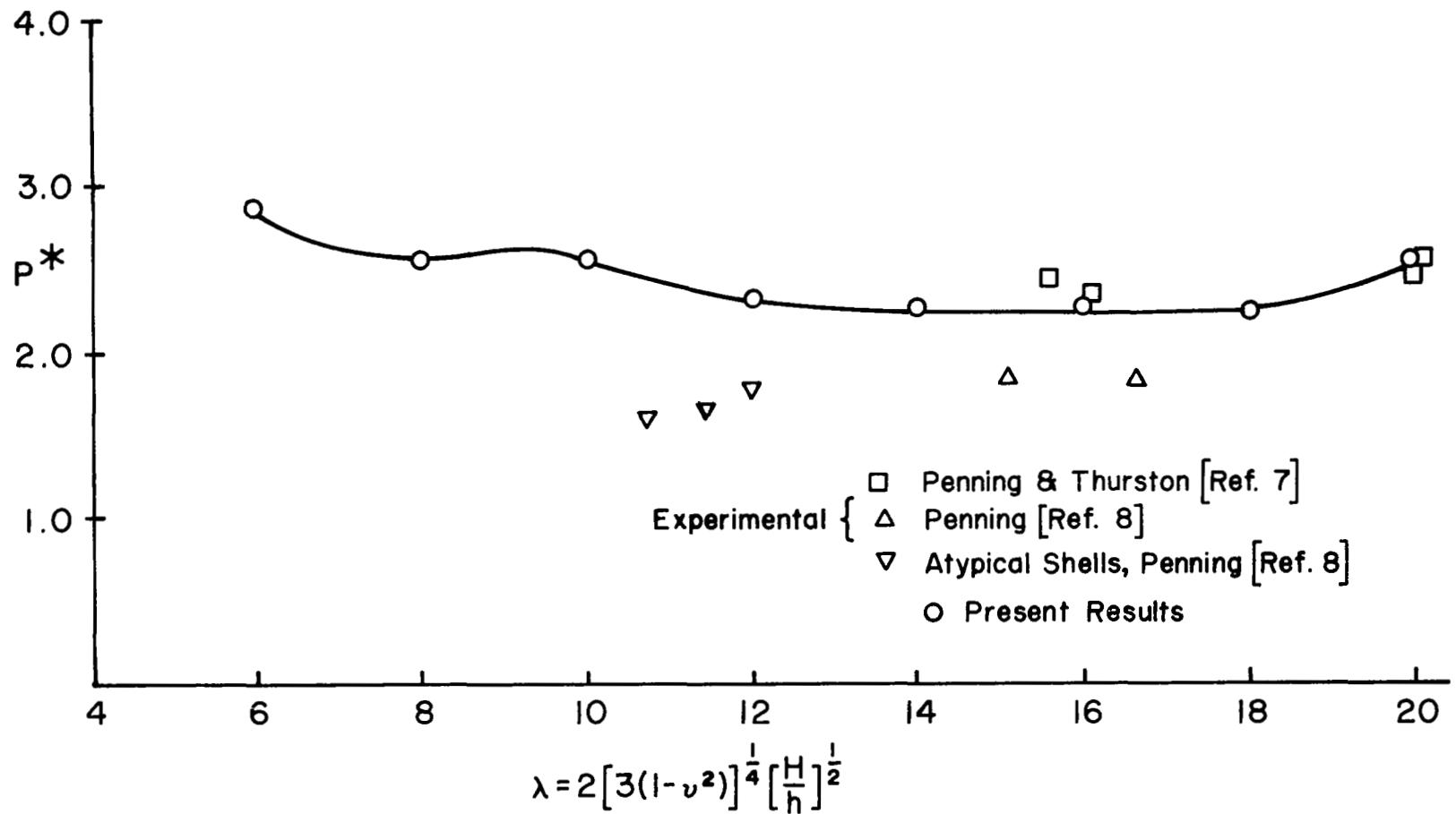


Fig. 12 Final loads for the axisymmetric behavior of clamped spherical caps under very small finite area loading at the pole.

in slope in the vicinity of $P^*=2.0$. Figure 13 shows the theoretical load-displacement curve for $\lambda=12$, and a reasonably accurate reproduction of the experimental results given in Ref. 8 for $\lambda=12.56$ and a small finite area load. Note that although the solution failed to converge for $P^* > 2.27$ snap buckling apparently is not imminent since the experimental results indicate that no snap occurs at this value of load, and the theoretical load-displacement curve does not show the significant decrease in slope that appears in Figs. 4 and 7 for the pressure loaded cap.

The results given in Fig. 12 indicate that snap buckling or a significant decrease in the slope occurs at approximately the same value of load for all values of λ considered. There appears to be a reasonable explanation for this since the experimental and theoretical results show the region of buckling to be in the neighborhood of the pole. For large values of λ , the outer boundary has very little effect on the behavior at the pole. As λ is reduced, the outer boundary moves closer to the pole and appears to reduce the severity of the snap, until finally, when $\lambda < 15$, it disappears. However, the localized nonlinear effect is still present and shows up as a decrease in slope of the load-displacement curve.

The final loads due to axisymmetric behavior for $\lambda=12$ and various values of $\bar{\lambda}$ are given in Fig. 14. As $\bar{\lambda}$ increases, and the load covers more of the shell's surface, the load-displacement behavior exhibited the softening behavior typical in Figs. 4 and 7.

b. Bifurcation Buckling

The final loads for asymmetric behavior for $\lambda=12$ and various values of $\bar{\lambda}$ are presented in Fig. 14 with the results obtained by Fitch and Budiansky. The load is given by equation (13) with $\epsilon=.0002$. The critical modes were selected from Ref. 6. For $\bar{\lambda} < 2.0$ the final loads

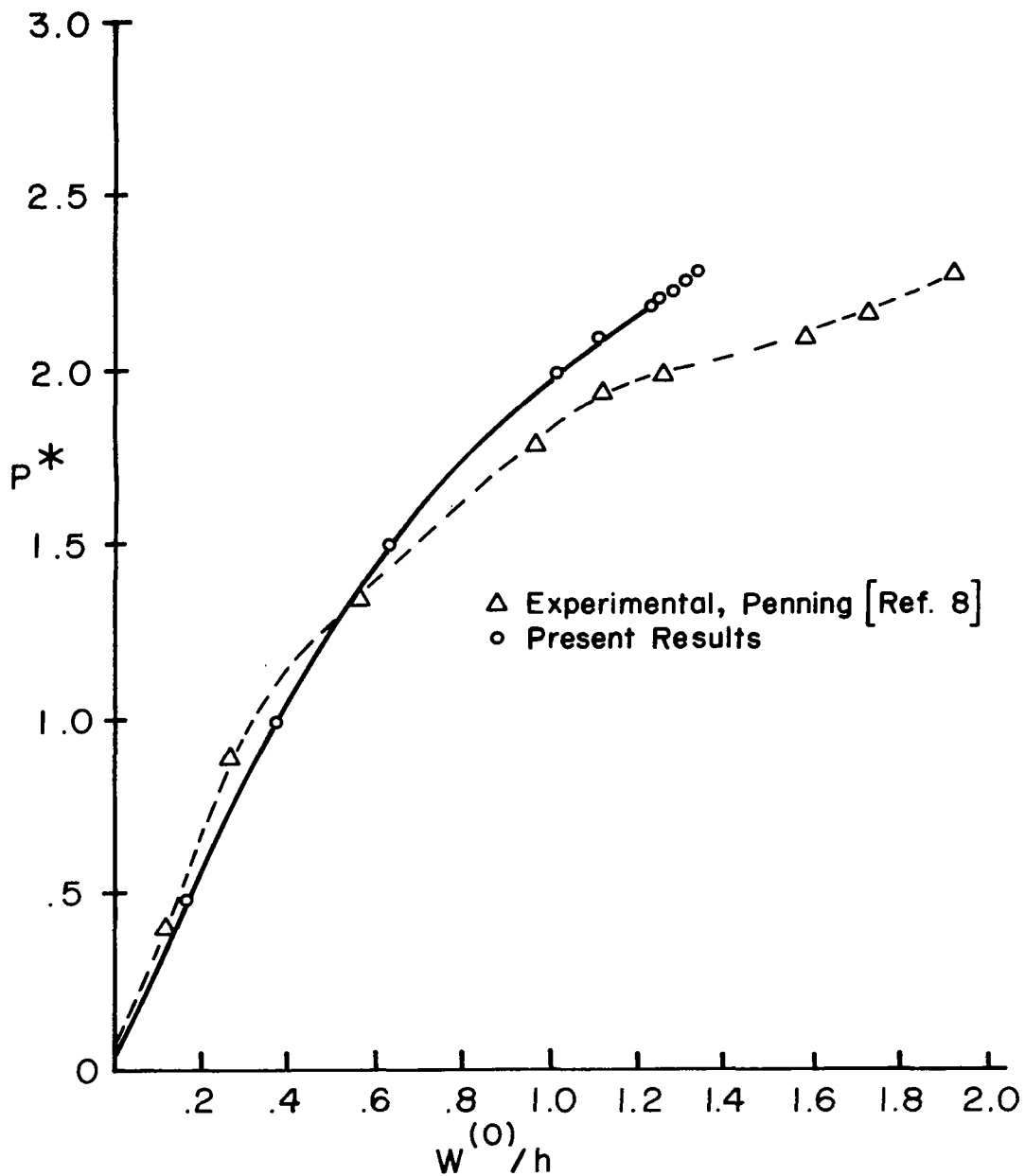


Fig. 13 Displacement at the pole of a clamped spherical cap, $\lambda = 12$, subjected to a small finite area load versus load.

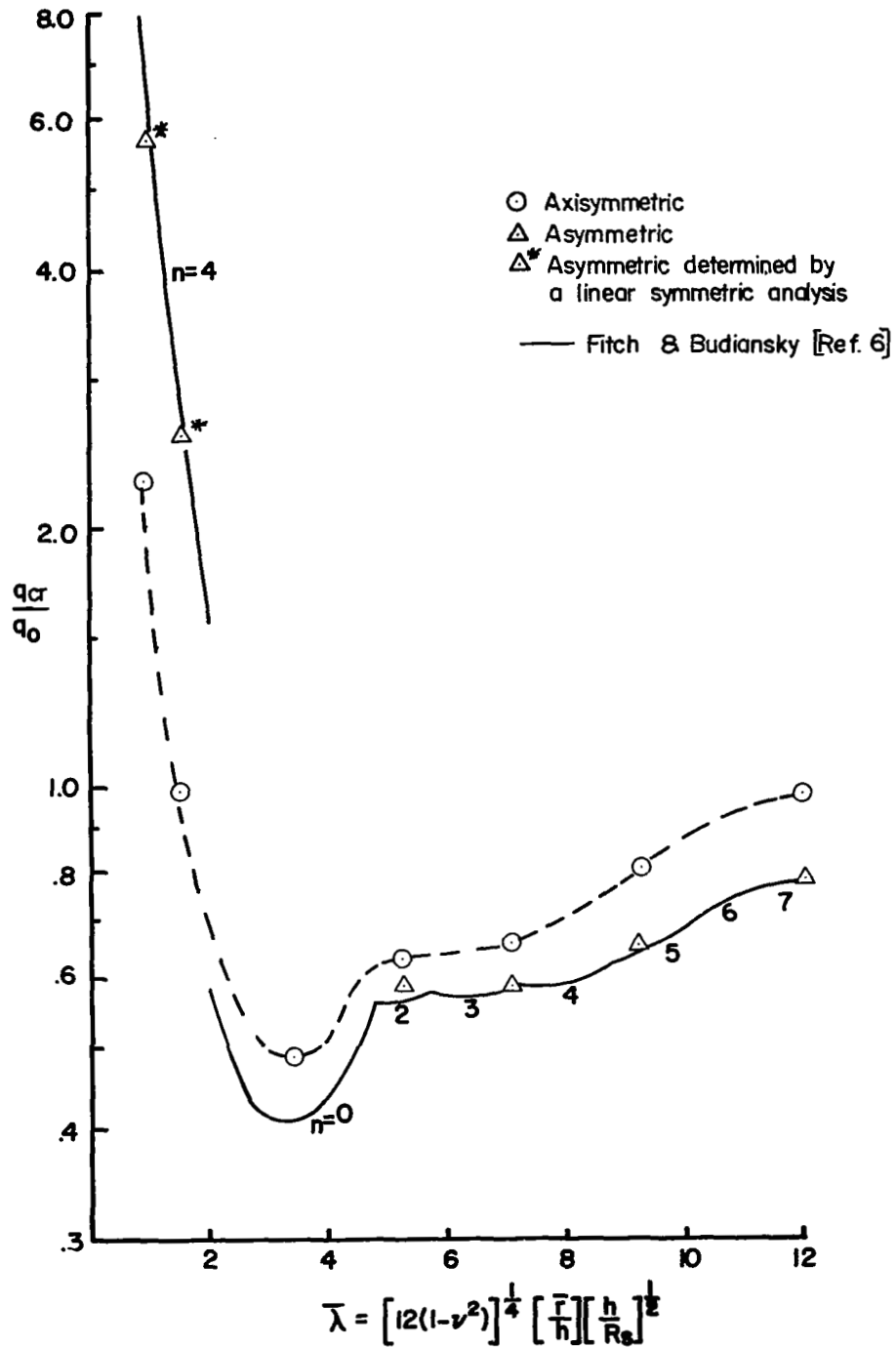


Fig. 14 Final loads for the axisymmetric and asymmetric behavior of a clamped spherical cap, $\lambda=12$, under finite area loading as determined by $\bar{\lambda}$

were obtained using a linear solution in the axisymmetric mode since the nonlinear axisymmetric solution failed to converge for loads much smaller than the bifurcation loads obtained by Fitch and Budiansky.

c. Imperfection Sensitivity

Results for the imperfection sensitivity of the shell $\lambda=12$ given in Ref. 6 show that for $\bar{\lambda} > 5$ the shell is imperfection sensitive, but for $\bar{\lambda} < 2$ the load increases after bifurcation and hence, the shell is insensitive. This latter feature is supported by the experimental results given in Refs. 7 and 8 where shells were observed to transition into the asymmetric mode shape without a noticeable loss of load carrying capacity.

It was not possible to use the program to determine the sensitivity for $\bar{\lambda} < 2$ since the solution failed to converge due to strong nonlinear behavior in the axisymmetric mode at loads much lower than the bifurcation loads⁶.

⁶As discussed in Section III.C., the use of a linear solution in the axisymmetric mode eliminates the ability of the program to determine sensitivity.

V. TRUNCATED HEMISPHERE DESCRIPTION AND RESULTS

A. GEOMETRY

Figure 15 shows the geometry of the truncated hemisphere. The values of the parameters used to describe two different shells are as follows:

	<u>Shell A</u>	<u>Shell B</u>
Radii of curvature, R_s, R_o	= 120 in	151 in
Thickness, h	= .24 in	.10 in
Included angle, ϕ_o	= 23.3 deg	23.2 deg
Modulus of elasticity, E	= 30×10^6 psi	
Poisson's ratio, ν	= .3	

B. LOAD DESCRIPTION

1. Axisymmetric

As shown in Fig. 15, an axisymmetric axial load $P_o / \cos \phi_o$ was applied to the top edge of the shell. For this loading condition, the reaction load at the lower boundary is P_o .

2. Asymmetric

Two types of asymmetric loads were used; one was a small perturbation in the axial load $\delta P_o \cos(N\theta) / \cos \phi_o$, and the other was a small uniform pressure $\epsilon q_o \cos(N\theta)$, where q_o is given by equation (7). Since the axial load was introduced as a boundary condition, and since the program considered the boundary conditions to be the same in every mode, some modifications had to be made to the program to allow a δ different from 1. The appropriate statements that allow a variable δ are presented in Appendix C.

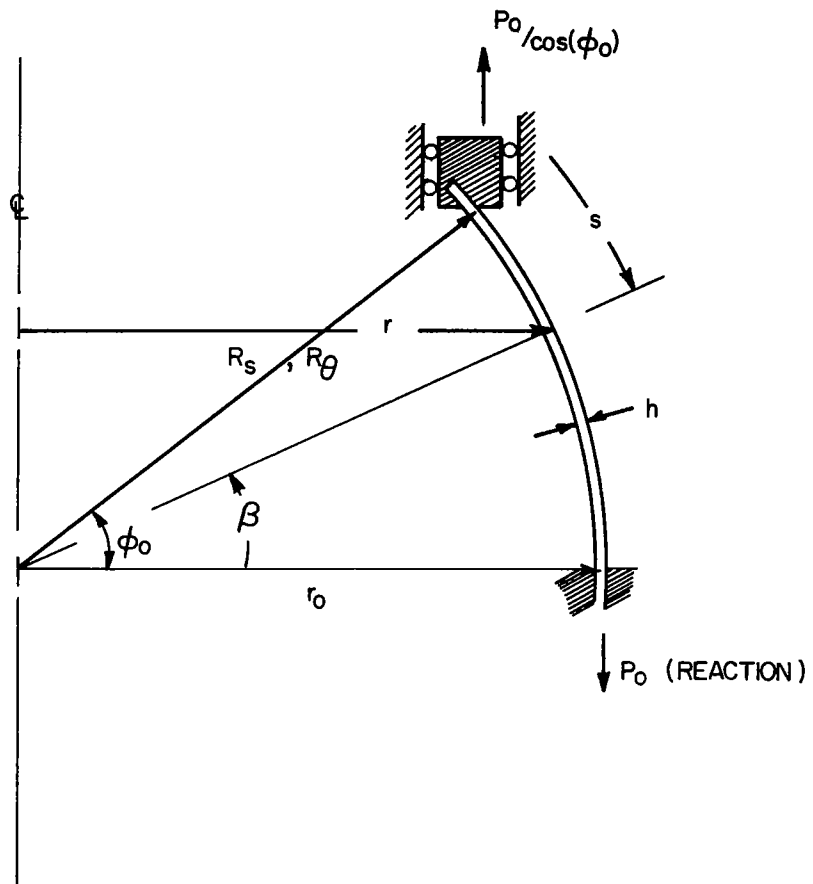


Fig. 15 Geometry of the truncated hemisphere

C. BOUNDARY CONDITIONS

The boundary conditions imposed on the shell at the top edge were

$$N_s \cos \theta_0 - Q_s \sin \theta_0 = P_0 \quad (15a)$$

$$U \sin \theta_0 - W \cos \theta_0 = 0 \quad (15b)$$

$$V = 0 \quad (15c)$$

$$\phi_s = 0 \quad (15d)$$

where N_s is the membrane force per unit length, and Q_s is the transverse force per unit length.

At the reaction end the shell was clamped, and the boundary conditions are given by equation (14).

D. PROCEDURES

A forty point finite difference net was used in all cases, and the convergence criterion was .01. The nonlinear axisymmetric behavior for the two shells was first obtained. Both types of asymmetric loads were then introduced, and the final loads, mode shapes and load-displacement curves were obtained for a linear and a nonlinear solution in the axisymmetric mode. The sensitivity of shell B was examined by varying both δ and ϵ .

E. RESULTS

1. Axisymmetric Behavior

The linear and nonlinear parts of the radial displacements at the final load are shown in Fig. 16 for shell A. The final displacement state of shell B was similar. Figure 17 depicts the load-displacement behavior for a station near the top of the shell where maximum stiffening occurred. Since Fig. 16 shows that there are no softening nonlinearities, failure of the solution to converge is attributed to the stiffening nonlinear

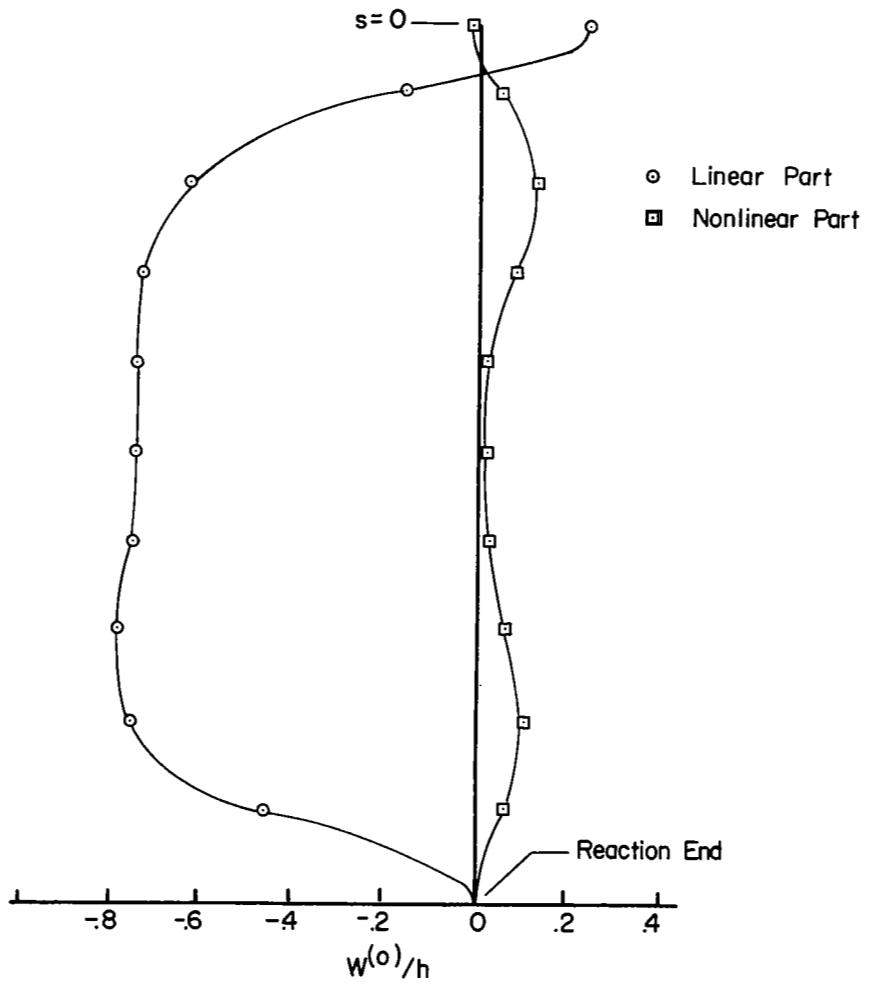


Fig. 16 Axisymmetric, normal displacements of Shell A under axial tension $P_o/Eh=1.325 \times 10^{-3}$

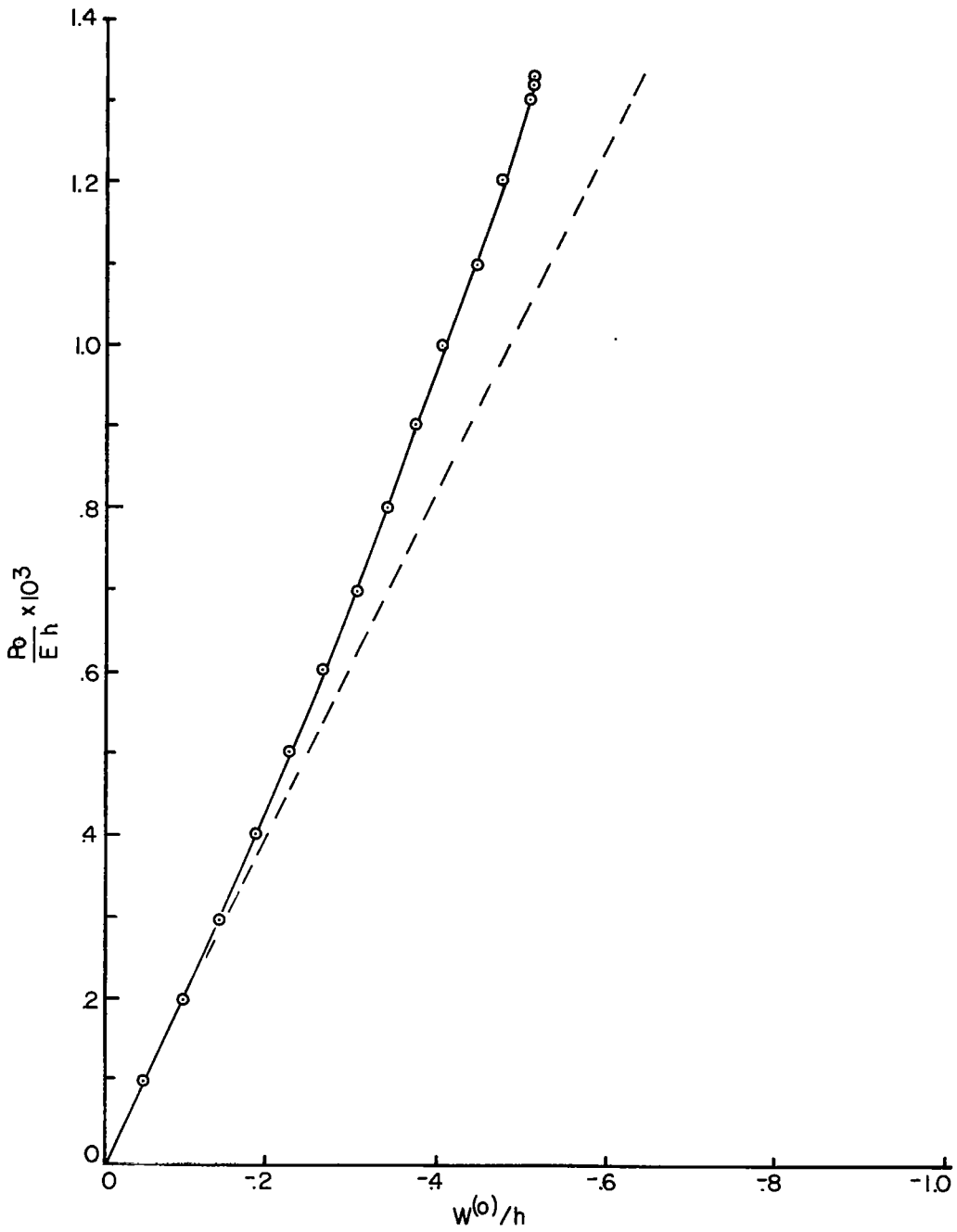


Fig. 17 Axisymmetric displacement, at station 8, versus load for Shell A

behavior. The final nondimensional load P_0/Eh was 1.325×10^{-3} for shell A and $.600 \times 10^{-3}$ for shell B.

2. Bifurcation Buckling

a. Shell A

The theoretical results obtained for the bifurcation loads versus mode number and the experimental buckling load given by Yao [Ref. 9] are presented in Fig. 18. Yao's theoretical results are based on a linear, membrane prebuckling assumption. Also shown in Fig. 18 are the present results obtained for the final loads using a linear symmetric analysis with an asymmetric load in the appropriate mode and $\delta=.0001$. Figure 19 presents the buckling mode shape for $N=40$ and $\delta=.0001$, and the mode shape assumed by Yao. The linear portion of the displacements was negligible at all stations along the meridian, and the requirements for a bifurcation analysis are satisfied. Similar results were obtained for $N > 30$.

For $N < 30$, the results for the final loads differ significantly from the bifurcation loads predicted by Yao. Figure 20 shows the modal displacements along the meridian at the final load for $N=15$ and $\delta=.0001$. Examination of Fig. 20 reveals that the linear part of the solution is larger than the nonlinear part, and that there is stiffening in the region near the applied load. Hence, the solution does not satisfy the conditions for a bifurcation analysis, and therefore, the final loads obtained for the lower mode numbers do not represent a critical load condition.

The values of the final loads were also obtained using a nonlinear symmetric solution. Figure 21 shows the nonlinear and linear parts of the modal displacements at the final load for $N=40$ and $\delta=.0001$.

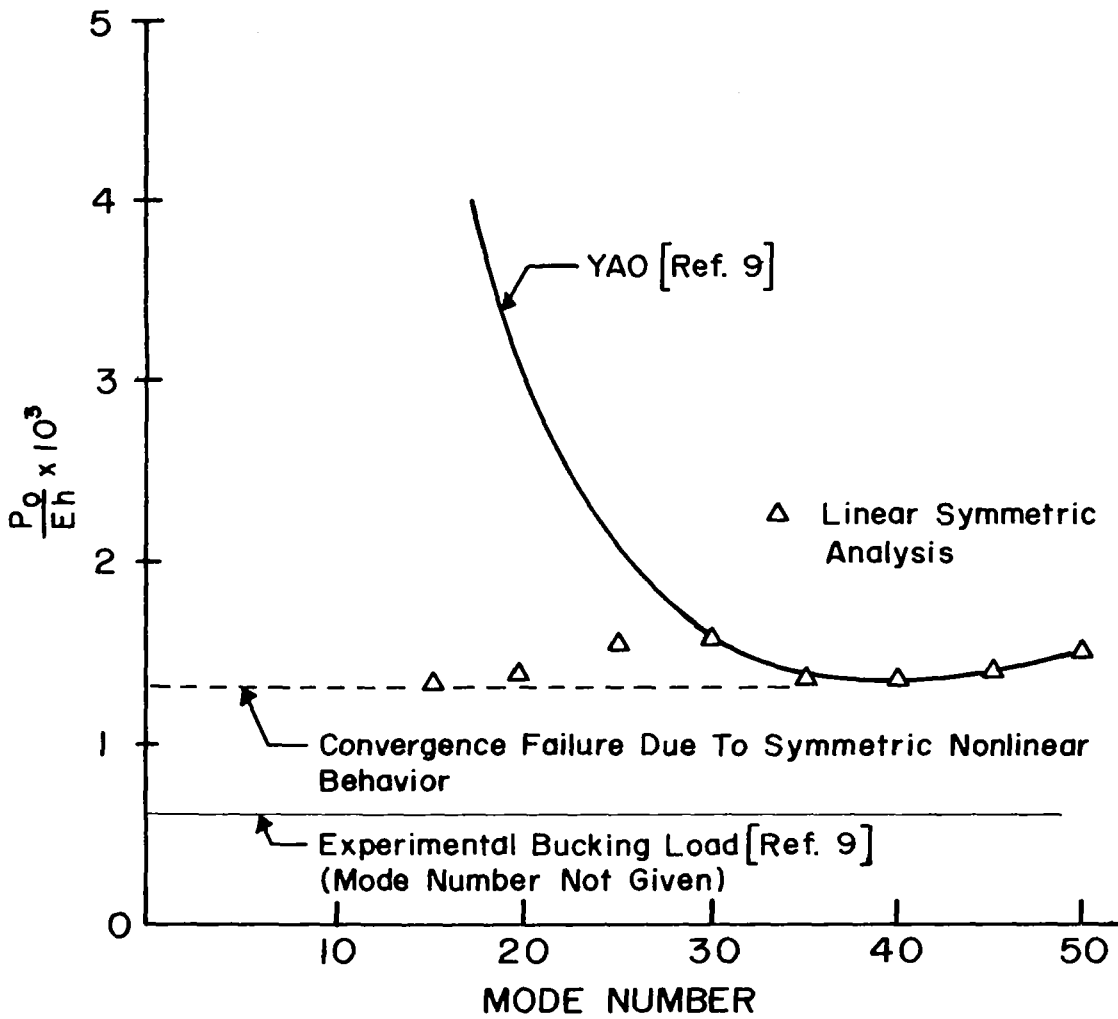


Fig. 18 Final loads for asymmetric behavior of Shell A subjected to axial tension with small asymmetric load, $\delta = .0001$

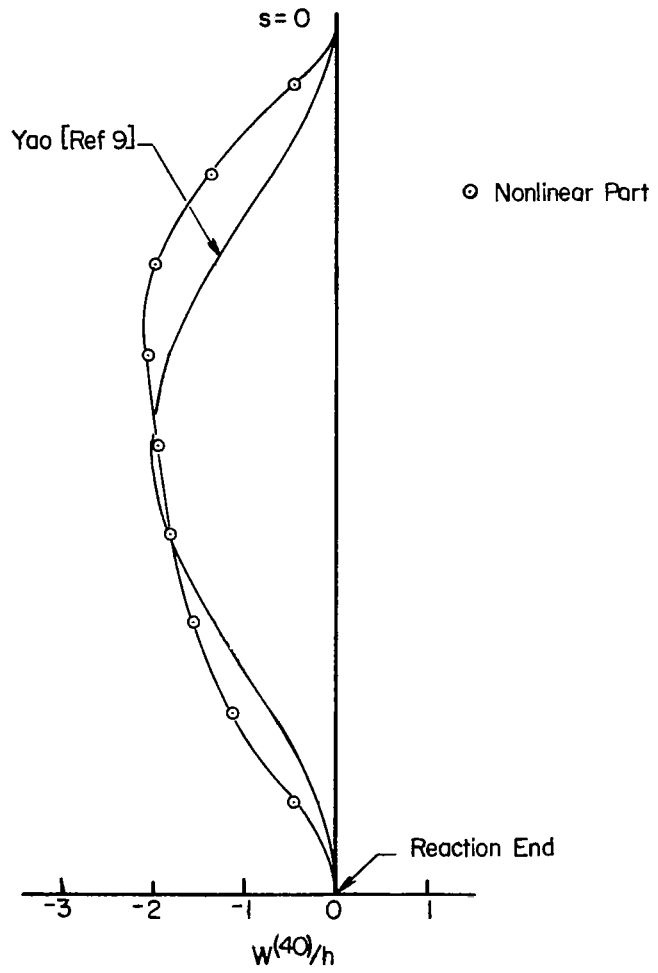


Fig. 19 Buckling, meridional mode shape, $N=40$, of Shell A subjected to axial tension with small asymmetric load, $\delta=.0001$

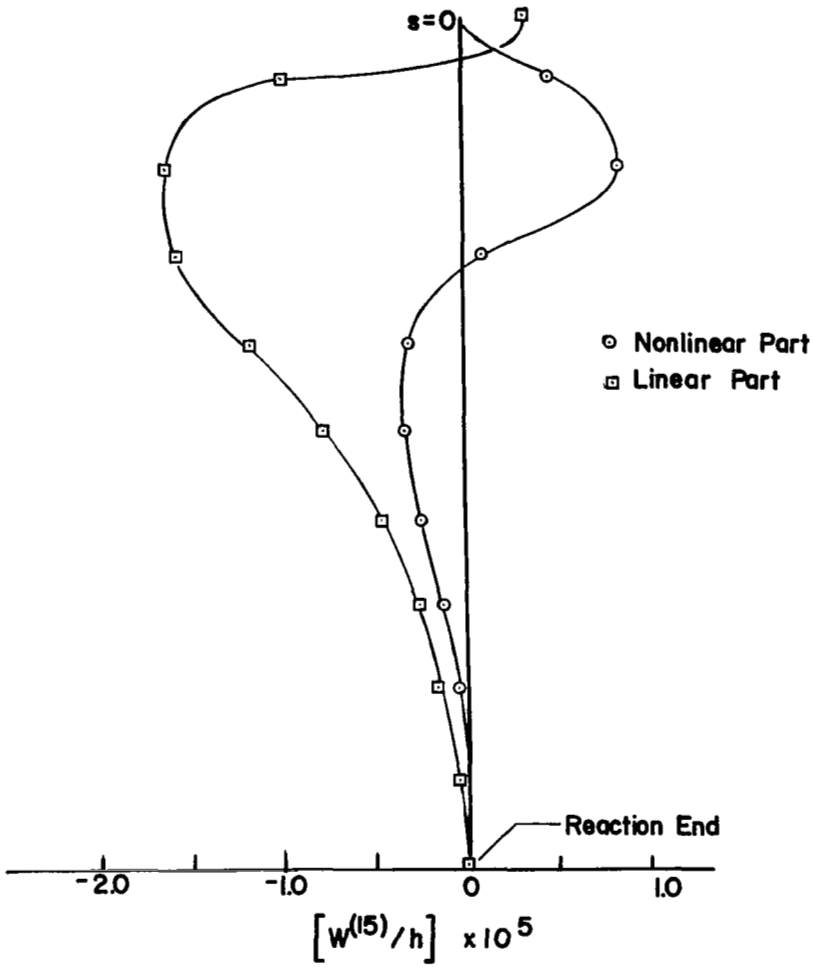


Fig. 20 Meridional mode shape, $N=15$, of Shell A subjected to axial tension with small asymmetric load, $\delta=.0001$

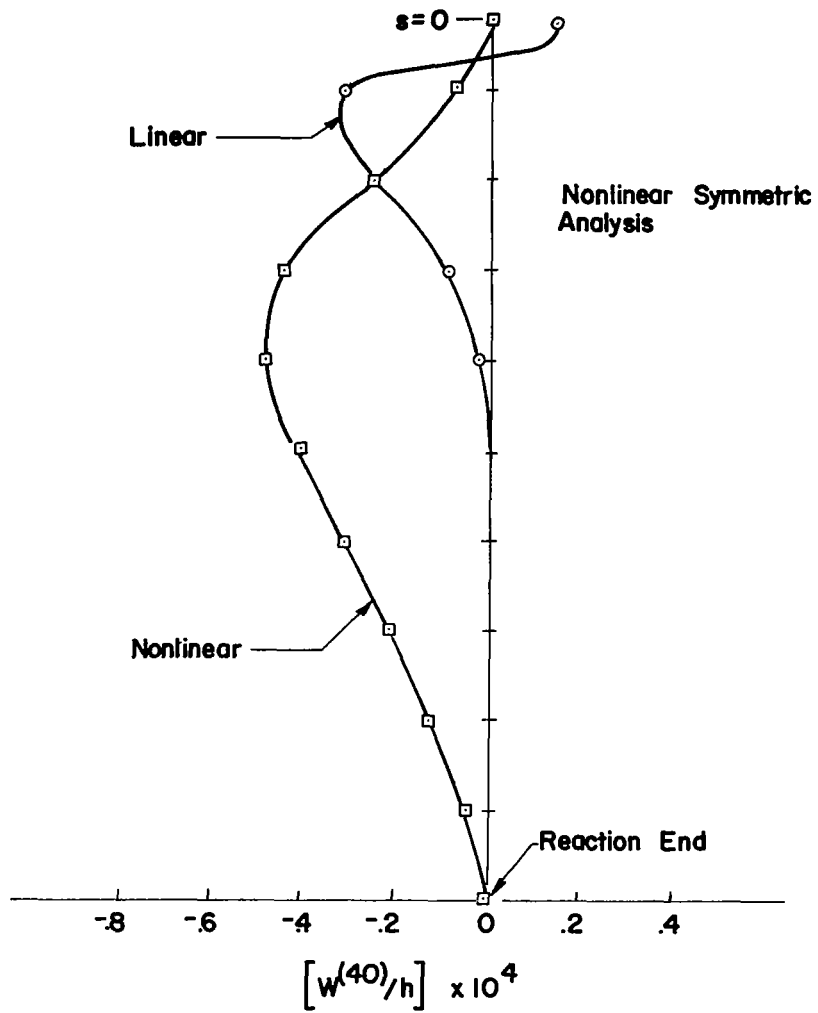


Fig. 21 Development of buckling mode shape, $N=40$, of Shell A subjected to an axial tension load in the vicinity of the critical load with small asymmetric load, $\delta=.0001$

Note that a mode shape is emerging, but the conditions for bifurcation analysis are only satisfied over that part of the shell where the linear displacements are negligible. Furthermore, convergence failure could not be definitely associated with either the asymmetric or the axisymmetric behavior since the final load for axisymmetric nonlinear behavior and the bifurcation load are approximately equal.

b. Shell B

The axisymmetric, nonlinear behavior of shell B did not experience convergence failure until the load was much larger than the minimum bifurcation load predicted by Yao. As a consequence, results were obtained for the final loads using a linear and nonlinear symmetric analysis with an asymmetric load in the appropriate mode and $\delta=.0001$. The results are presented in Fig. 22 along with the theoretical bifurcation loads and experimental buckling load presented in Ref. 9.

Figure 23 shows the nonlinear part of the modal radial displacements at the final load for $N=70$, $\epsilon=.001$, and a nonlinear symmetric analysis. The linear part of the modal displacements were negligible at all stations and the mode shape is essentially the same as the mode shape for shell A shown in Fig. 19. Although the solution was obtained using a nonlinear symmetric analysis, failure of the solution to converge could definitely be associated with the asymmetric behavior.

For $N < 35$ final loads were obtained below the bifurcation loads predicted by Yao. As was the case for shell A, the solutions at these lower mode numbers did not satisfy the conditions for a bifurcation analysis.

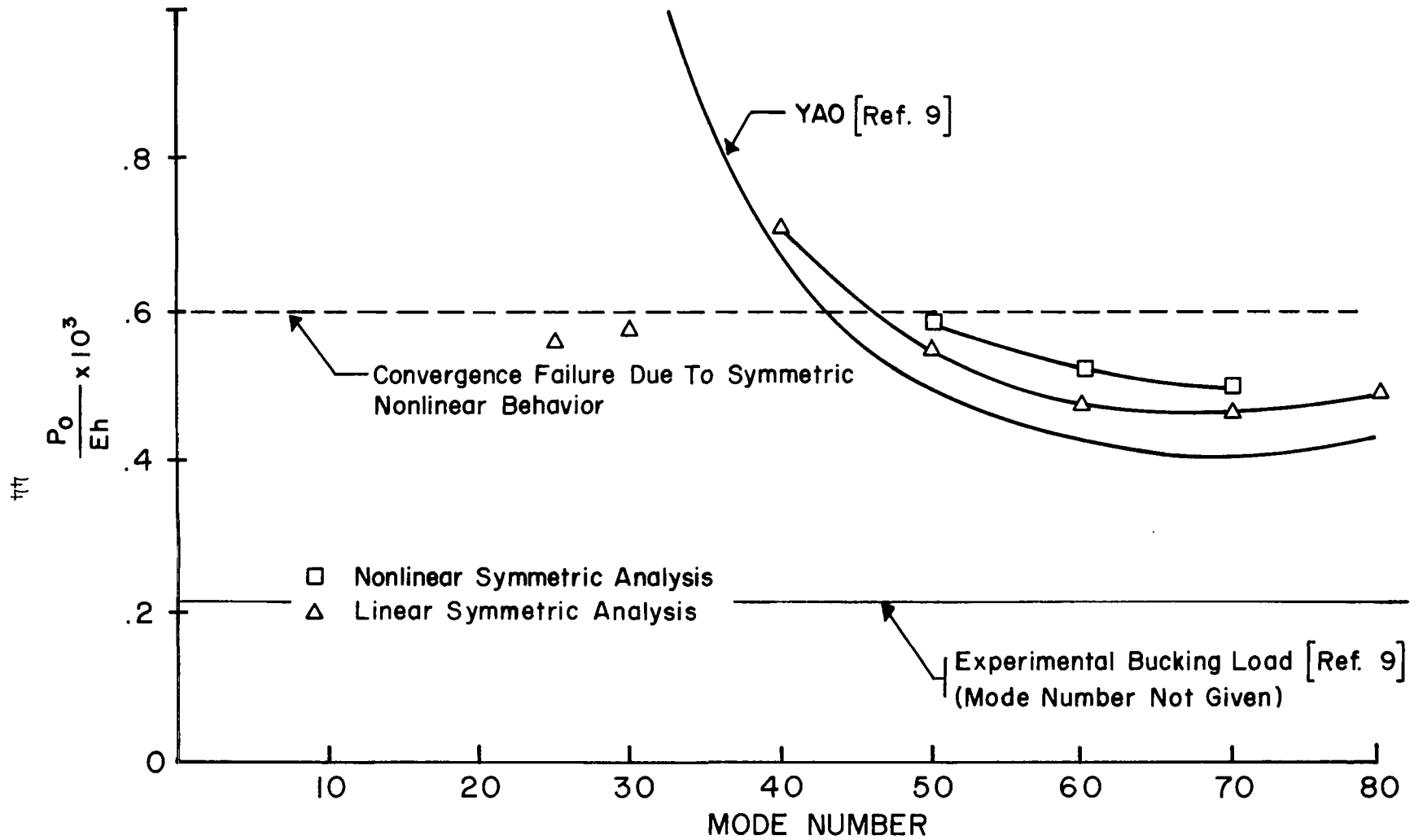


Fig. 22 Final loads for asymmetric behavior of Shell B subjected to an axial tension with small asymmetric load, $\delta = .0001$

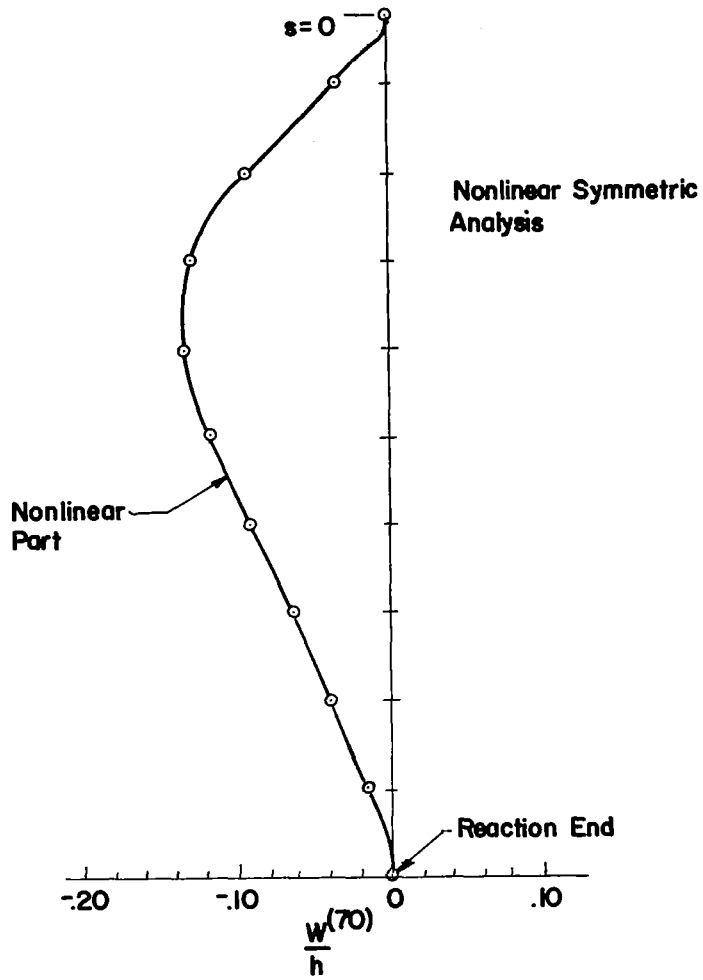


Fig. 23 Buckling, meridional mode shape, $N=70$, of Shell B subjected to an axial tension with small asymmetric pressure, $\epsilon=.001$

3. Imperfection Sensitivity

The sensitivity of shell A could not be examined since a linear axisymmetric solution was required for the bifurcation analysis.

The sensitivity of shell B for $N=70$ was examined using an asymmetric axial load $\delta P_0 \cos(N\theta) / \cos \theta_0$ and an asymmetric pressure load $\epsilon q_0 \cos(N\theta)$. The variation of final load with respect to δ and ϵ is shown in Fig. 24. For the asymmetric axial load, the final load was constant as the magnitude of δ was increased. However, examination of Fig. 21 reveals that the asymmetric axial load causes linear displacements only in the region near the applied load. Outside this region the linear displacements are effectively zero⁷. Therefore, the use of an asymmetric axial load does not introduce linear displacements of any consequence away from the region near the applied load. On the other hand, the use of an asymmetric pressure load introduces linear displacements over the entire region of the shell and is considered more applicable for examining sensitivity.

Figure 25 shows the effect of the asymmetric pressure load upon the final load and axisymmetric displacement at station twenty. The behavior at all stations in the central region of the shell is exemplified by the behavior at station twenty. For $\epsilon < .01$, there was a small decrease in the final load and a small increase in the final axisymmetric displacement. However, for $\epsilon = .10$, there was a significant reduction in the final load, and the final axisymmetric displacement is approximately the same as that associated with $\epsilon = .01$. This type of behavior is similar to that obtained for the spherical cap under uniform pressure.

⁷Since the net axial load in the asymmetric mode is zero, the linear modal stresses become smeared as the distance from the load application is increased. Thus, there is little or no asymmetric stress present at the reaction end.

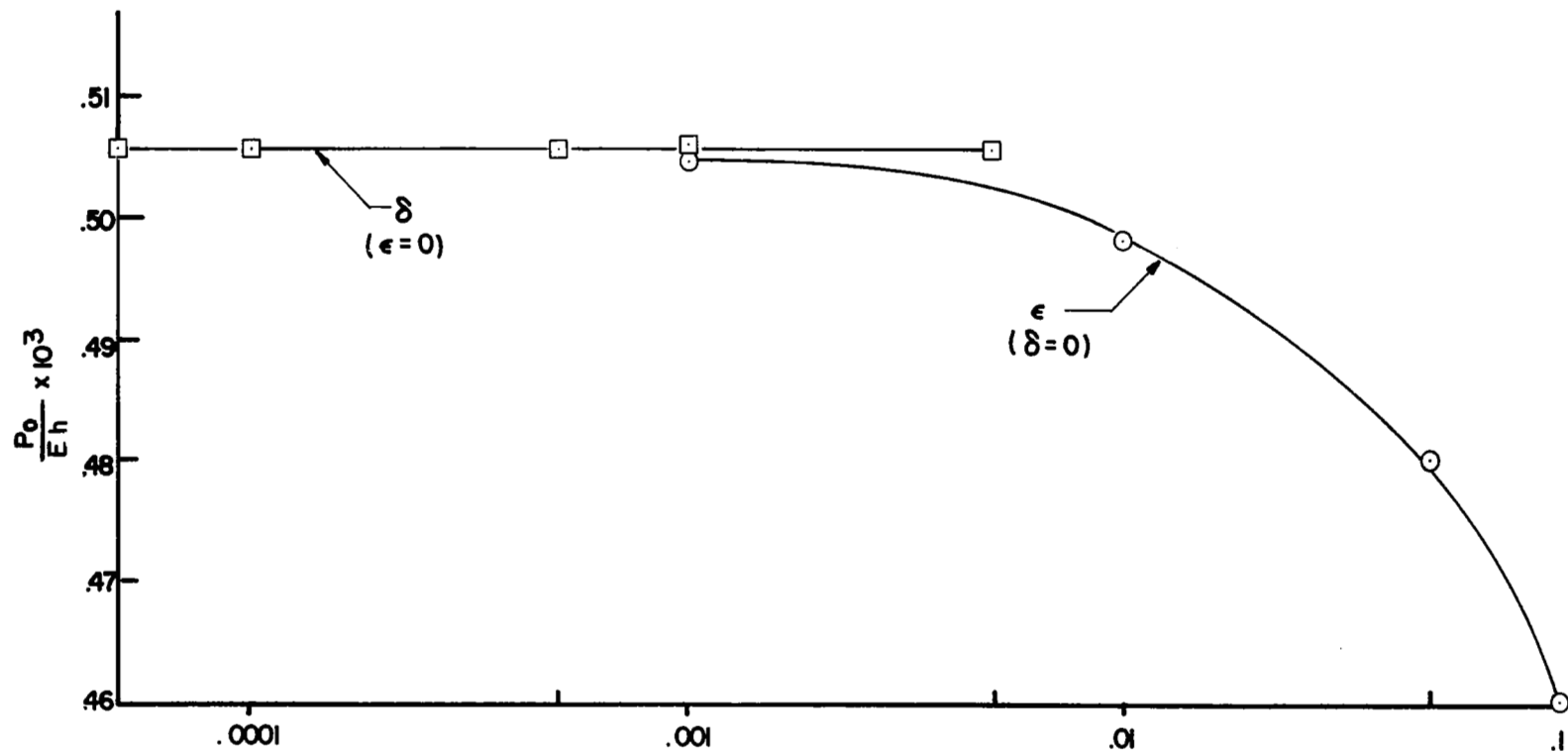


Fig. 24 Variation of final load with δ and ϵ for Shell B

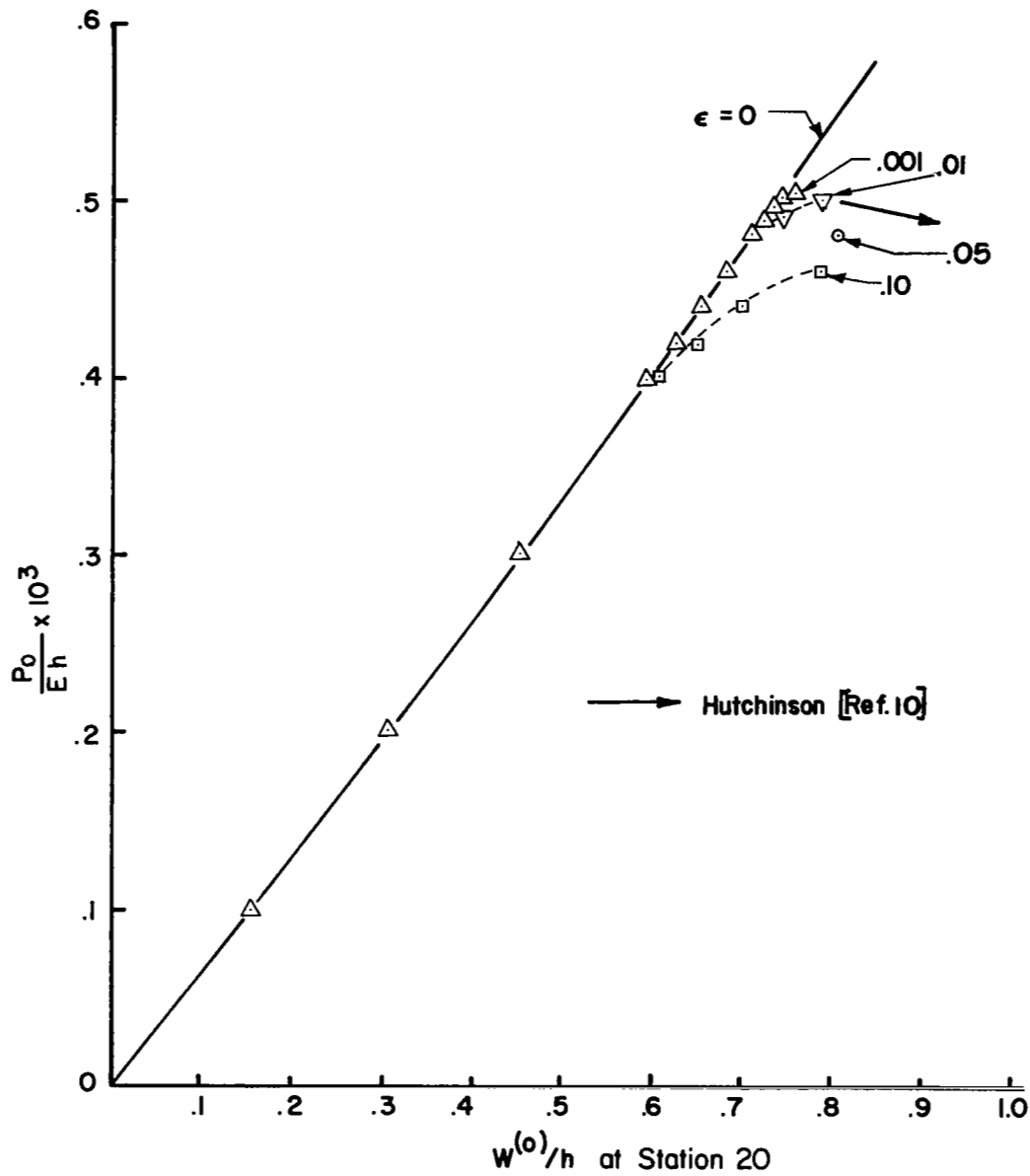


Fig. 25 Sensitivity of Shell B to load imperfections

Hutchinson [Ref. 10], in an analytical study of the initial postbuckling of toroidal shells, suggested that the imperfection sensitivity of Yao's truncated hemispheres should agree qualitatively with the degree of sensitivity that he obtained for the simply supported hemispherical segments subjected to axial tension. Shells A and B fall within the imperfection sensitive range predicted by Hutchinson. A plot of the initial slope of the generalized load-deflection curve⁸, as given in Ref. 10, for the perfect toroidal shell corresponding to shell B is shown in Fig. 25.

⁸Hutchinson's load-displacement plot is based on axial elongation. An appropriate conversion was applied to his slope to account for differences in nondimensionalization.

VI. CONCLUSIONS

A. FINAL LOADS AS BUCKLING LOADS

As a consequence of the method of solution used in the computer program, the solution may fail to converge for both softening and stiffening nonlinearities. Thus, a careful examination of the solution should be made before proclaiming a final load to be a buckling load. For axisymmetric snap buckling, the load-displacement curves should indicate that a region of nearly zero slope has been reached. For bifurcation buckling loads, the above should hold true for the modal displacements, and the linear part of the modal displacements must be negligible compared to both the nonlinear part of the modal displacements and the axisymmetric displacements.

There are instances when it's not completely clear why the solution fails to converge. For example, consider the results obtained for very small finite area loads on a clamped spherical cap. For $\lambda > 15$, the experimental results indicate that an axisymmetric snap occurs at an approximate value of load for which the computer solution failed to converge. However, for $\lambda < 15$ the solution experienced convergence problems at loads where the slope changed significantly, but no snap buckling occurred. Archer [Ref. 11] obtained similar theoretical results for simply supported caps using the pseudo load approach. Mescall [Ref. 12] notes that Archer's final loads were loads for which the numerical procedure could not converge and were not due to the existence of a maximum on the load-displacement curve. Throughout this study an attempt has been made to clarify this point. In those cases where the results

did not indicate the existence of a maximum on the load-displacement curve, the final loads were not classified as buckling loads.

B. AXISYMMETRIC SNAP BUCKLING

1. Spherical Cap

The results obtained for the axisymmetric snap buckling loads of the spherical cap under uniform pressure compare favorably with previously published theoretical results. Since the load-displacement curve shows the approaching region of zero slope associated with the existence of a maximum and snap buckling, and since convergence failure can definitely be attributed to this softening nonlinear behavior, the classification of the final loads as snap buckling loads is considered justified.

The case of small area loading, approaching a point load, gave results for high rise caps that compare favorably with experimental results. The load-displacement behavior indicated that snap buckling was imminent. At smaller values of λ , the behavior is not characterized by indications that a maximum exists on the load-displacement curve, and failure of the solution to converge is not associated with snap buckling, but with moderate changes in stiffness of the shell.

As the area of loading is increased, the behavior is again characterized by the type of nonlinear behavior indicative of snap buckling and the final loads obtained are considered to be snap buckling loads.

2. Truncated Hemisphere

Final loads were obtained for the axisymmetric behavior of the truncated hemisphere under axial tension. However, these loads do not represent critical loads, but are the last value of the load for which a solution could be obtained. Failure of the solution to converge is attributed to stiffening nonlinearities.

C. BIFURCATION BUCKLING

The results of the investigation of asymmetric behavior under nearly axisymmetric load indicate that the program can be used to predict bifurcation buckling loads. In fact, the results obtained for the bifurcation loads using the asymptotic procedure are better than was anticipated, since an extremely small disturbance in the mode is all that is required to trigger nonlinear modal displacements that are much larger than the linear modal displacements as the load approaches a critical value.

1. Spherical Cap

The bifurcation loads obtained for the spherical cap for all loading conditions are in very good agreement with previously published theoretical results. For an asymmetric load with a maximum magnitude of .01% to .05% of the axisymmetric load, the linear asymmetric displacements are negligible compared to the axisymmetric displacements and the nonlinear asymmetric displacements are negligible until the applied load reaches a value within 95% of the final load. The buckling mode shapes compare favorably with previous results.

2. Truncated Hemisphere

The bifurcation loads obtained for the truncated hemisphere are in good agreement with the previously published theoretical results, and the critical mode numbers are in excellent agreement. Several final loads were obtained for low mode numbers that do not agree with the previous results, but these loads are easily eliminated as bifurcation loads.

D. IMPERFECTION SENSITIVITY

The sensitivity of a given shell and loading condition to imperfections is a result of the nature of the modal coupling between the axisymmetric

mode and the asymmetric modes. When the failure of the solution to converge can definitely be attributed to softening nonlinearities in the asymmetric mode, the computer program can be used to determine the coupling effects and the sensitivity can be estimated.

1. Spherical Cap Under Uniform Pressure

For the pressure loaded cap with $\lambda=8$, reductions in the final load with increasing magnitude of imperfections are accompanied by reductions in the final value of the axisymmetric displacements. Furthermore, the failure of the solution to converge is due to softening nonlinearities in the asymmetric mode. Therefore, this pressure loaded cap shows a strong sensitivity to imperfections. This conclusion is in agreement with the previous theoretical analysis given in Ref. 6.

2. Truncated Hemisphere Under Axial Tension

The axisymmetric behavior of the truncated hemisphere under axial tension shows stiffening over the entire region of the shell, and the solution encounters convergence problems due to this stiffening. Nevertheless, the final load for shell B, subjected to a very small asymmetric load in the critical mode, is a bifurcation load, and a sensitivity analysis of this shell is possible. For increasing values of asymmetric axial load there is no change in the final load. This is due to the fact that the imperfections in the axial load generate displacements and stresses only in the upper region of the shell. In this region, the asymmetric displacements have negligible effect upon the axisymmetric displacements, and the shell appears to be imperfection insensitive. On the other hand, an asymmetric pressure load causes displacements over the entire shell. For very small values of ϵ , less than .01, the asymmetric mode does have some effect on the axisymmetric mode; the final load is slightly reduced

but the final displacements in the axisymmetric mode are increased. Thus, the shell is sensitive to small imperfections, but the behavior differs from that of the spherical cap. For larger imperfections the asymmetric mode has a pronounced effect upon the axisymmetric behavior in the central region of the shell, and there is a significant reduction in the value of the final load with virtually no change in the final value of the axisymmetric displacements. This type of behavior is similar to that of the spherical cap.

Hutchinson [Ref. 10] suggested that the imperfection sensitivity of Yao's shells should agree qualitatively with the degree of imperfection sensitivity he obtained for simply supported hemispherical segments. Reference 13 contains a summary of the results of Hutchinson's study and a discussion on the postbuckling coefficient used to determine sensitivity. The imperfection sensitivity of circular cylindrical shells under axial compression is used as a calibration for the significance of the postbuckling coefficient. Based on Hutchinson's prediction, shell B is not as sensitive to imperfections as the cylinder or the spherical shell, but it does fall in a region where a significant reduction in the buckling load may occur.

The present results for small ϵ are in agreement with Hutchinson's prediction. However, for larger ϵ the results indicate an apparent change in the nature of the sensitivity and the behavior resembles that of the spherical cap. Since the experimental buckling loads of shells A and B are about one half of the theoretical bifurcation loads, which is common for pressure loaded spherical caps, this analysis appears to offer a reasonable explanation for the large discrepancy between the bifurcation loads and the experimental buckling loads.

APPENDIX A

USER PREPARED SUBROUTINES

The following are user prepared subroutines necessary to describe the stiffness, geometry and loads for the various shells examined in this study. Certain input parameters were required before calculation of any quantities in the subroutines. These values were input into the main part of the program.

KMAX - total number of meridional stations
MNMAX - the number of terms used in the expansion of the applied load
NU - Poisson's ratio (ν)
ELAST - reference modulus of elasticity (E_o)
TKN - reference thickness (h_o)
CHAR - characteristic length (a)
SIGO - reference stress (σ_o)

A. STIFFNESS

The stiffness quantities necessary in the program are calculated at each meridional station (K) by subroutine BDB. The nondimensional form of the Fortran variables for a homogeneous, isotropic, constant thickness shell are as follows:

$$B = \frac{\int E d\zeta}{E_o h_o (1-\nu^2)} = \frac{1}{(1-\nu^2)} \quad (E = E_o, h = h_o)$$

$$D = \frac{\int E \zeta^2 d\zeta}{E_o h_o^3 (1-\nu^2)} = \frac{B}{12}$$

$$DB = \frac{dB}{ds} = 0$$

$$DD = \frac{dD}{ds} = 0$$

Since all the shells examined were assumed to be homogeneous, isotropic and constant thickness, only one subroutine was required.

```

SUBROUTINE BDB(K,B,DB,D,DD)
REAL NU
COMMON
1/BL32/TKN,ELAST,CHAR,SIGO/BL15
2/NU,U1(10),V1(10),W1(10),V2(10),U2(10),W2(10),U3(10),
3V3(10),W3(10)
B=1./(1.-NU**2)
D=B/12.
DB=0.
DD=0.
RETURN
END

```

B. GEOMETRY

The geometric quantities necessary in describing the shells are defined in subroutine GEOM. The following are the nondimensional Fortran variables required at each meridional station (K).

$$\text{DEL} = \frac{S}{(K\text{MAX}-1)a}$$

$$R(K) = \left[\frac{r}{a} \right] K$$

$$\text{GAM}(K) = \left[\frac{dr/ds}{r} \right] K$$

$$\text{OMT}(K) = \left[\frac{a}{R_e} \right] K$$

$$\text{OMXI}(K) = \left[\frac{a}{R_s} \right] K$$

$$\text{DEOMX}(K) = \frac{d}{ds} \left[\frac{a}{R_s} \right] K$$

1. Spherical Cap

Prior to calling subroutine GEOM, certain quantities were input or calculated in MAIN and are as follows:

FCTZ = λ	(input)
CHAR = $R_s = R_o$	(input)
HTR = H^s	(calculated)
FCTL = S	(calculated)
RL = r_o	(calculated)

The necessary statements in MAIN required for calculating the desired quantities are as follows:

```
HTR=TKN*(FCTZ**2)/SQRT(58.*(1.-NU**2))
RL=SQRT((2.*CHAR*HTR)-(HTR**2))
FCTL=CHAR*ARSIN(RL/CHAR)
```

Subroutine GEOM is as follows:

```
SUBROUTINE GEOM
COMMON
1/IBL4/KMAX,KL
0/BL8/R(200),GAM(200),OMT(200)
3/BL11/OMXI(200),PHEE,TO,T2
4/BL17/DEL
4/BL20/DEOMX(200)
6/BL32/TKN,ELAST,CHAR,SIGO
RK=KMAX-1
DEL=(FCTL/RK)/CHAR
DO 4 K=2,KMAX
RK=K
THET=(RK-1.)*DEL
R(K)=SIN(THET)
GAM(K)=COS(THET)/R(K)
OMT(K)=1.
OMXI(K)=1.
4 DEOMX(K)=0.
R(1)=0.
GAM(1)=0.
OMT(1)=1.
OMXI(1)=1.
DEOMX(1)=0.
RETURN
END
```

2. Truncated Hemisphere

The input quantities required in MAIN are as follows:

PHIO = ϕ_o	(input in radians)
CHAR = $R_s^o = R_o$	(input)

Subroutine GEOM is as follows:

SUBROUTINE GEOM

(COMMON STATEMENTS)

```

RK=KMAX-1
DEL=PHIO/RK
DO 13 K=1,KMAX
RK=K-1
BETA=PHIO-(RK*DEL)
R(K)=1.-(1.-COS(BETA))
GAM(K)=SIN(BETA)/R(K)
OMT(K)=COS(BETA)/R(K)
OMXI(K)=1.
13 DEOMX(K)=0.
RETURN
END

```

C. LOAD

The axial loading case is covered in Appendix C and the pressure loading case is described in the following.

The reference pressure loads for each coefficient used in the cosine expansion of the load, at each meridional station, were calculated or defined in subroutine PLOAD. The following are the nondimensional Fortran variables required

$$\begin{aligned}
 NN(I) &= n \\
 PR(I) &= \frac{aq^n}{\sigma_o h_o}
 \end{aligned}$$

For the shells examined, the following reference values were used and were input or calculated in MAIN.

MOD1	- the first asymmetric mode number used in load	
	description	(input)
CHAR	= a = R = R _e	(input)
TKN	= h = h ^s	(input)
SIGO	= $\sigma_o = q_o$	(calculated)

The statement required to calculate SIGO is

$$SIGO=(2.*ELAST*TKN)/(CHAR*SQRT(3.*(1.-NU**2)))$$

1. Spherical Cap

The load description for the spherical cap, in all cases, required a symmetric pressure load and, for the majority of runs, one or more modal pressure loads. The symmetric mode ($n=0$) was always NN(1) and PR(1) was equal to -1. corresponding to an external pressure. A Fortran variable, FCTR, was an input parameter determining the number of stations loaded and was equal to KMAX for the uniform load. The magnitude of the asymmetric load was governed by the input variable EPSL.

The subroutine PLOAD for the spherical cap is as follows:

```
SUBROUTINE PLOAD(K)
COMMON/BL32/TKN,ELAST,CHAR,SIGO/IBL2/NN(10),MNINIT
8/BL6/Z(4,220),SOE,OSE,ALOAD/IBL1/MNMAX
5/BL3/PR(10),PX(10),PT(10)/IBL4)KMAX,KL
6/BL8/R(200),GAM(200),OMT(200)/BIL2/EPSL,MOD1,LINA
M=MOD1-2
DO 10 I=1,MNMAX
10 NN(I)=M+I
   NN(1)=0
   IF(K.GT.FCTR) GO TO 39
   DO 11 I=1,MNMAX
11 PR(I)=EPSL
   PR(1)=-1.
   GO TO 40
39 DO 12 I=1,MNMAX
12 PR(I)=0.
40 RETURN
END
```

2. Truncated Hemisphere

For the truncated hemisphere the only pressure load used was an asymmetric load in one mode, and PR(1) was always equal to zero. The Fortran parameter EPSL was used to govern the magnitude of the asymmetric axial load and the magnitude of the asymmetric pressure load was specified within subroutine PLOAD. If an asymmetric axial load was used then PR(2) was set equal to zero. Subroutine PLOAD for the truncated hemisphere is as follows:

SUBROUTINE PLOAD(K)

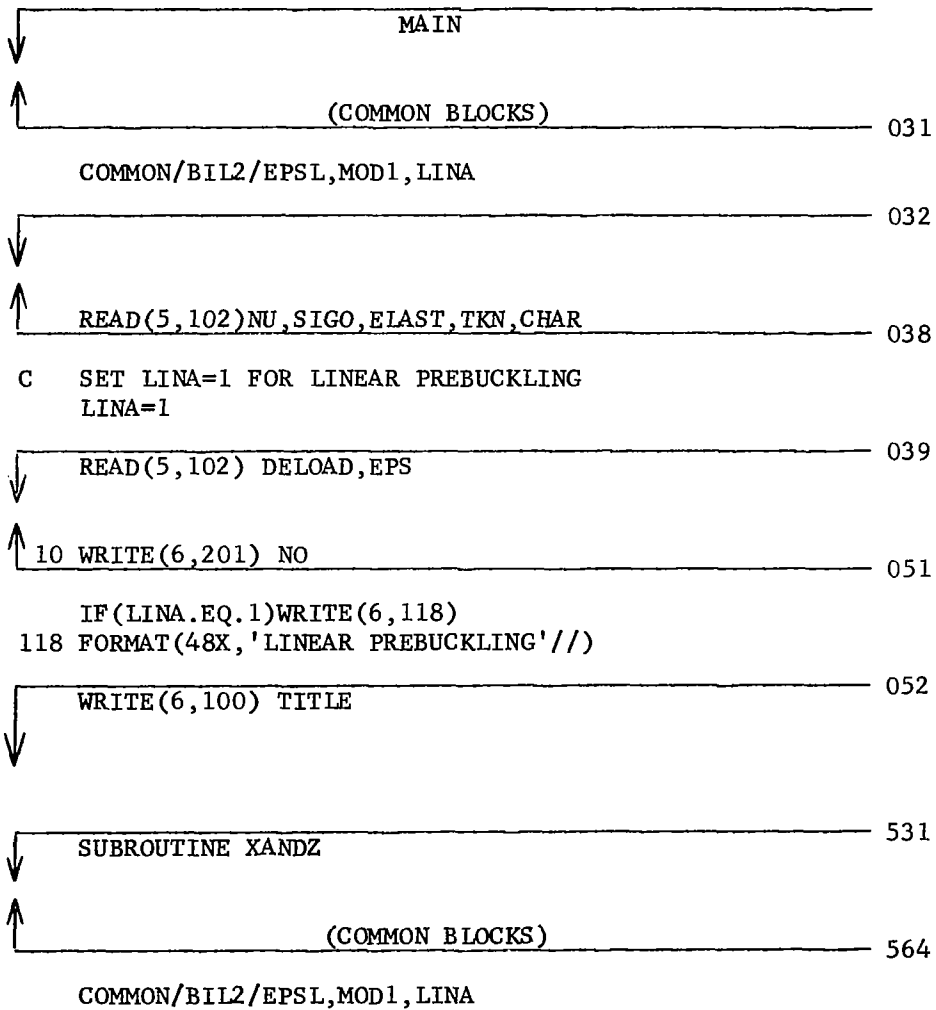
(COMMON STATEMENTS)

NN(1)=0
NN(2)=MOD1
PR(1)=0.
PR(2)=-.001
RETURN
END

APPENDIX B

ADDITIONS TO THE PROGRAM FOR LINEAR SYMMETRIC SOLUTION

The following is a listing of the statements and their location within the various sections of the program that allowed the nonlinear terms in the symmetric mode to be by-passed and the linear solution obtained.



```

565
↓
↑ DO 8 M=1,MNMAX 622
CALL TLOAD(1) 623

IF(M.EQ.1.AND.LINA.EQ.1) GO TO 7

FFS(1,M)=-TT(M)*ALOAD+OSE*(BX1(M)....ETC... 624
FFS(2,M)=OSE*(B1 *D1 *BST1(M)....ETC... 625
FFS(3,M)=LAM2*GAM1*D1*MT(M)*ALOAD-...ETC... 626

GO TO 8
7 FFS(1,M)=0.
FFS(2,M)=0.
FFS(3,M)=0.

8 FFS(4,M)=0. 627
↓
↑ DO 14 M=1,MNMAX
CALL TLOAD(KMAX) 650

IF(M.EQ.1.AND.LINA.EQ.1) TO TO 11

FLS(1)=-TT(M)*ALOAD+OSE*(BX3(M).....ETC... 651
FLS(2)= OSE*(B1*D1*BXT3(M)+EX3.....ETC... 652
FLS(3)=LAM2*GAM1*D1*MT(M)*ALOAD.....ETC... 653

GO TO 13
11 FLS(1)=0.
FLS(2)=0.
FLS(3)=0.

13 IK=KL+KMAX*(M-1) 654
↓

SUBROUTINE FORCE(K) 960
↓
↑ (COMMON BLOCKS) 987

COMMON/BIL2/EPST,MOD1,LINA

988
↓
↑ EX2T=EX2(M) 066
ET2T=ET2(M) 067

7 IF(LINA.EQ.1.AND.M.EQ.1) TO TO 31

```

```

GEE(1)=GEE(1)*OSE*(BS*(DBX+DBE+GA*.....ETC... 068
2      (EXT2T+ETT2T))*TDEL 076
31 IF(K.GT.1) GO TO 10
DO 20 I=1,4 078
SUBROUTINE OUTPUT(IMODE) 445
      (COMMON BLOCKS) 473
COMMON/BIL2/EPSL,MOD1,LINA
TTS=TT(MN)*ALOAD 474
IF(MN.EQ.1.AND.LINA.EQ.1) GO TO 13
EX=(U3(MN)-U1(MN))*TDLI +OX*W2(MN) + ..... ETC ... 522
1 + ENL*SOE*BXT3(MN) 525
GO TO 14
13 EX=(U3(MN)-U1(MN))*TDLI+OX*W2(MN)
    ET=ENR*V2(MN)+GA*U2(MN)+OT*W2(MN)
    EXT=.5*((V3(MN)-V1(MN))*TDLI-ENR*U2(MN)-GA*V2(MN))
14 KT=ENR*PHIT(MN)+GA*PHIX(MN) 526
KXT=.5*(ENR*(-PHIX(MN) -GA*W2(MN) + (W3.....ETC... 527
CALL TLOAD(K) 851
TTS=TT(MN)*ALOAD 852
IF(MN.EQ.1.AND.LINA.EQ.1) GO TO 15
EX=(U3(MN)-U1(MN))*TDLI +OX*W2(MN).....ETC... 853
1 + ENL*SOE*BXT3(MN) 856
GO TO 16
15 EX=(U3(MN)-U1(MN))*TDLI+OX*W2(MN)
    ET=ENR*V2(MN)+GA*U2(MN)+OT*W2(MN)
    EXT=.5*((V3(MN)-V1(MN))*TDLI - ENR*U2(MN)-GA*V2(MN))
16 KT=ENR*PHIT(MN)+GA*PHIX(MN) 857

```

↓ $KXT = .5 (ENR * (OPHX (MN) * GA * W2 (MN) + (W3 (MN) \dots \dots ETC \dots))$ 858

APPENDIX C

ADDITIONS TO THE PROGRAM FOR ASYMMETRIC AXIAL LOAD

In order to adjust the magnitude of the asymmetric axial load, additional logic was incorporated in subroutines XANDZ and FORCE. The axial loads are entered as boundary conditions and are described by the Fortran variables EL1S and ELLS. A Fortran variable EPSL was used to determine the magnitude of the asymmetric load and is contained in the COMMON block BIL2, which was introduced in Appendix B. The symmetric part of the load was always taken as the first mode, described by NN(1)=0. The necessary statements required are as follows:

SUBROUTINE XANDZ	531
↓	
DO 14 I=1,4	657
SUMZ=0.	658
↑	
DO 15 J=1,4	659
IF(M.EQ.2.AND.I.EQ.1) ELLS(J)=ELLS(J)*EPSL	
15 SUMZ=SUMZ+ZFIM(I,J,M)*.....ETC...	660
↓	
SUBROUTINE FORCE(K)	960
↑	
DO 21 J=1,4	081
IF(M.EQ.2.AND.I.EQ.1) EL1S(J)=EL1S(J)*EPSL	
21 SUMX=SUMX+DL(I,J,M)*EL1S.....ETC...	082
↓	

LIST OF REFERENCES

1. Bushnell, David, Computer Analysis of Shell Structures, paper presented at the Winter Annual Meeting of the ASME, Los Angeles, California, 16-20 November 1969.
2. National Aeronautics and Space Administration Contractor Report 909, A Geometrically Nonlinear Analysis of Arbitrarily Loaded Shells of Revolution, by R. E. Ball, January 1968.
3. National Aeronautics and Space Administration Technical Report D-3926, Computer Program for Finite-Difference Solutions of Shells of Revolution under Asymmetric Loads, by Harry G. Schaeffer, May 1967.
4. Weinitschke, H. J., "On Asymmetric Buckling of Shallow Spherical Shells", Journal of Mathematics and Physics, v. 44, p. 141-163, June 1965.
5. Huang, Nai-Chien, "Unsymmetrical Buckling of Thin Shallow Spherical Shells", Journal of Applied Mechanics, v. 31, p. 447-457, September 1964.
6. Fitch, J. R. and Budiansky, B., "Buckling and Postbuckling Behavior of Spherical Caps under Axisymmetric Load", AIAA Journal, v. 8, no. 4, p. 686-693, June 1970.
7. National Aeronautics and Space Administration Contractor Report 265, The Stability of Shallow Spherical Shells under Concentrated Load, by F. A. Penning and G. A. Thurston, July 1965.
8. Penning, F. A., "Experimental Buckling Modes of Clamped Shallow Shells under Concentrated Load", Journal of Applied Mechanics, v. 33, p. 297-304, June 1966.
9. Yao, J. C., "Buckling of a Truncated Hemisphere under Axial Tension", AIAA Journal, v. 1, p. 2316-2320, October 1963.
10. Hutchinson, J. W., "Initial Post-Buckling Behavior of Toroidal Shell Segments", International Journal Solids Structures, v. 3, p. 97-115, 1967.
11. Archer, R. R., "On the Numerical Solution of the Nonlinear Equations for Shells of Revolution", Journal of Mathematics and Physics, v. XLI, p. 165-178, September 1962.
12. Mescall, J. F., Large Nonsymmetric Deflections of Thin Shells of Revolution, paper presented at Proceedings of the Army Symposium on Solid Mechanics, Johns Hopkins University, Baltimore, Maryland, September 1968.
13. Budiansky, B. and Hutchinson, J. W., "A Survey of Some Buckling Problems", AIAA Journal, v. 4, p. 1505-1510, September 1966.